Report.

Research projects of the FEhS-Institute **2022**

INSTITUT FÜR BAUSTOFF FORSCHUNG

FEhS

ADVANCED SOLIDIFICATION SYSTEM FOR TRANSFERRING HOT LADLE FURNACE SLAG TO AN ELECTRIC ARC FURNACE TO REPLACE LIME AND RECOVER HEAT

A. Morillon, PhD; D. Algermissen, M.Sc.
(FEhS – Building Materials Institute)
Dr.-Ing. D. Mudersbach; S. Schüler, B.Eng.
(Max Aicher Umwelt GmbH, Meitingen)

ABSTRACT

To overcome logistical barriers to charging liquid ladle furnace (LF) slag into an electric arc furnace (EAF) to recycle LF slag as lime substitute and recover energy from the slag, an advance solidification system, using the "sandwich" concept, was developed during the RFCS ECOSLAG project. The sandwich concept is based on tapping of LF slag/metal from multiple heats into an intermediary vessel (tundish in the case of the project), which can then be transported to the EAF. The LF slag/metal sandwich temperature should be kept below the solidification temperature of the outside slag (below 1,000°C) but above the disintegration temperature of the LF slag (which was determined in the project to be 200°C). The results of laboratory LF slag temperature tests and industrial trials of the sandwich concept are presented in the article. The resulting EAF slag leaching analysis showed that recycling of the LF slag did not have a negative effect on the resulting EAF slag. However, the energy gain in the EAF with the sandwich addition was inconclusive due to too few trials, but additional energy consumption was also not observed. While the advance solidification system showed good potential, long term trials would need to be performed to understand how much lime can be replaced with LF slag and how much energy saving can be obtained from the liquid slag addition.

INTRODUCTION

Ladle furnace (LF) slag is an industrial by-product of secondary metallurgy to produce and refine high-quality steels. The crude steel from an electric arc furnace (EAF) is treated to achieve a specific quality by different additions, which results in the final steel product and LF slag. It is assumed that for every ton of steel, 1%–8% of LF slag is produced [1]. Since the EU produced 152.6 Mt of crude steel in 2021 [2], it can be estimated that at least 1.5 Mt of ladle slag was produced. The rate of LF slag utilization depends on the country and steelwork, but often it is not used and therefore landfilled. The LF recycling rate is limited because of the tendency of LF to disintegrate because of dicalcium silicate (C2S) disintegration, which is present in LF slag.

LF slag can be recycled internally or externally depending on its characteristics and opportunities around the steelwork. The opportunities will depend on the regulatory situation in a given area, the need and costs for primary resources, acceptance by a community and ease with which a steelwork can handle this material.

Some of the external LF slag utilization paths include use as liming material or in soil stabilization.

Internally, the liquid or solid LF slag can be recycled into an EAF as a substitute for lime with or without heat recovery depending on if it is done in liquid or solid form [3, 4]. The LF solid slag can also be charged into a blast furnace (BF) as a slag former [5]. Another example is for the LF slag to be added into the EAF slag to decrease V leaching; however, care has to be taken to ensure that the resulting EAF slag meets regulations [3, 6]. LF slag recharging into an EAF is practiced in a few steelworks in Europe. However, most of the steelworks do not have the logistical possibility of recharging liquid LF slag into an EAF or the

solidified LF slag disintegration makes it impractical for charging into an EAF due to dust issues.

Two previous RFCS projects investigated recycling LF slag into an EAF [7, 8].

Kuehn M. et al. investigated recycling LF slag in a liquid and solid state in industrial trials. The liquid LF slag was directly recycled from the LF pot into an EAF with successful results of reducing about 50%–80% of generated LF slag and saving 15% of lime over a 1-year period. A difference in energy consumption of up to 0.4% on average was noted, which was assumed to be due to heat radiation loss during roof opening. Kuehn M. et al. also examined the addition of solid LF slag to an EAF, as not all steelworks can handle adding liquid LF slag for various reasons (logistics, timing, etc.). Depending on the grain size of the LF slag, it can be either added by pneumatic injection or agglomeration of the fines before charging (e.g. pelletization). About 15% of lime was able to be substituted with the LF slag without changing the basicity of the resulting EAF slag and only minor effects were seen with respect to metallurgy and steel quality, while sulphur in the resulting EAF slag during the testing period was below the requirement.

Colla V. et al. (RFCS ERISS project) conducted a case study using the Aspen simulation tool to determine the environmental effects of recycling solid LF slag into an EAF, such as variation in input (LF slag, lime, energy) and output (waste and by-product generation, metallic yield, etc.). In the case study, it was concluded that additional energy would be needed to remelt the LF slag while generating a higher amount of EAF slag. However, with respect to an environmental point of view and the KPIs used, the addition of LF slag to the EAF process was better than the current process.

In order to deal with logistical issues at different steelworks, where direct charging of molten LF slag to an EAF is not possible and where solidified LF slag also cannot be incorporated into an EAF, this article presents the "sandwich concept", which was used to charge liquid LF slag into an EAF to recover heat and substitute lime from the LF slag as part of the RFCS ECOSLAG project "Eco-friendly steelmaking slag solidification with energy recovery to produce a high quality slag product for a sustainable recycling", from June 2018 to May 2022. The requirement was for LF slag to be kept solidified but before disintegration for the purpose of transportation while giving the steelwork time to charge the LF slag to the EAF when convenient for the process and not because the LF slag is ready. The concept involved creating a system where the LF pot can be tapped into a tundish from 2-5 heats of LF slag in an area where the LF pot can be transported, and the tundish shape can be used to charge the LF slag into the EAF while the slag is solidified but not disintegrated, to also maximize the heat recovery. Laboratory tests were done to investigate the disintegration temperature of the LF slag and industrial trials were conducted to test the logistics of the sandwich concept.

METHODS

Sandwich concept

As the LF slag pot cannot always be moved to the EAF as there are restraints to crane movement at some steelworks, a sandwich concept was investigated. The idea is to have a container, in this case a tundish, into which LF slag can be tapped, and the container can be used as an intermediary vessel. The LF slag might also contain different percentages of metal. The amount of time between the tapping and charging of the LF sandwich into te EAF is very important. The slag needs to solidify enough so that it can be taken out of the tundish and transported to the EAF, but not cooled enough to start disintegrating. The idea is to keep the slag as "hot" as possible to recover the maximum potential of the energy. Between each tapping, the metal in the slag has some time to separate from the slag. The result looks like a "sandwich" with layers of metal and layers of slag (Figure 1). Rods need to be inserted into the tundish during the solidification process so that they can be used to lift the solidified LF slag to charge it into the EAF.

Laboratory LF slag disintegration temperature tests

To understand at what temperature range the LF slag needs to be kept before it is added to the EAF (LF slag needs to be charged to the EAF after it solidifies, but before it starts to disintegrate, to avoid creating problems with dust), laboratory trials were conducted with 3 different LF slag samples from different steelworks (LFS1, LFS2 and LFS3) to measure at what temperature the slag starts to disintegrate. LF slag

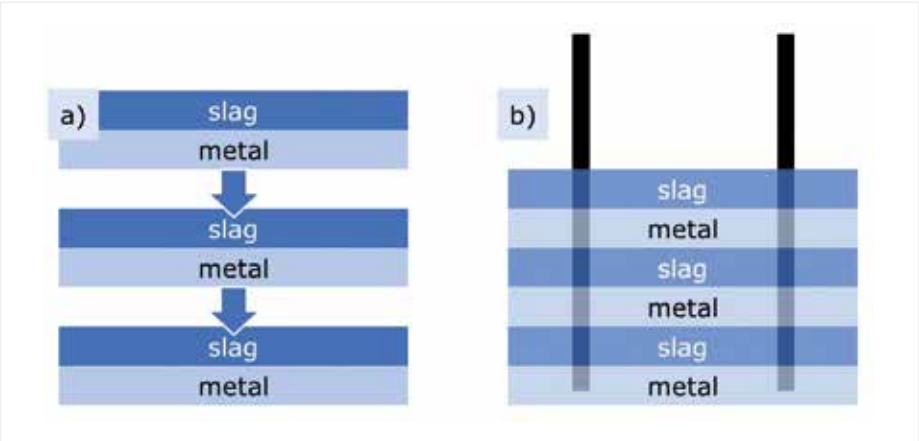

Figure 1: a) Separation of slag and metal in the tundish after 3 tappings; b) Rods used to take out the "sandwich" from the tundish

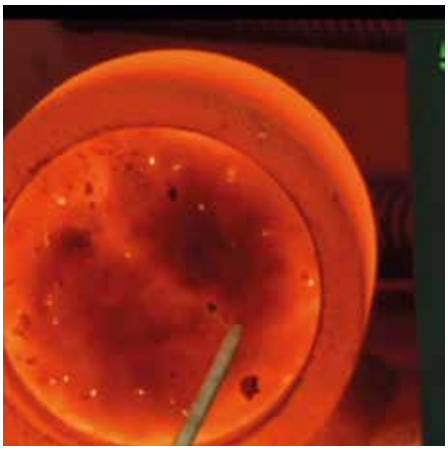

Figure 2: LF slag in a muffle furnace with a thermocouple at about 600°C

Figure 3: Recording of LF slag during cooling

Figure 4: LF slag in a muffle furnace with a thermocouple disintegrating during cooling

Figure 5: Tundish after lining with cement

(1,500 g) was placed in a carbon crucible and heated to 1,550°C in a Tammann furnace to ensure that all the slag melted. Once the temperature was reached, the crucible was cooled to about 1,000°C and moved to a muffle furnace where a thermocouple was inserted and the slag was cooled to about 600°C. Once the slag was cooled to about 600°C, it was placed on its side (Figure 2) and the door was left open a small gap during the cooling period so that the crucible could be recorded (Figure 3). At this temperature point, the slag did not spill out once the crucible was placed on its side. The cooling down of the slag was recorded and the temperature at which disintegration started was noted (Figure 4).

Industrial trials of the sandwich concept

The tundish used as an intermediary vessel was made of metal and was lined with refractory material (Figure 5), which can withstand not only layers of slag, but also metal. The tundish was large enough to handle up to 5 heats of LF slag/metal. During tapping, various amounts of metal were tapped together with the slag (sometimes if there are issues with the quality of the metal, more metal than slag is tapped).

Industrial trials were conducted with production of 4 sandwiches, which were charged to the EAF. Each time, the tundish was filled with 2 heats of LF slag and remaining steel, thereby creating a sandwich structure. Due to the timing and the available equipment, it was not possible to determine the exact mass of the sandwiches. Each time the tundish was brought to the tilting device, where typically the remaining material of the tundish falls out, before the tundish was used again. During the tests, the sandwich (LF slag and steel) fell out from the tundish without breaking (Figure 6).

Figure 6: Tilting of the tundish and falling out of the sandwich

Figure 7: Transporting the sandwich and hanging like a mobile

Figure 8: Charging the sandwich to the EAF

After this, the sandwich was transported by a forklift inside the steelwork, in the line of the scrap baskets. Steel rods were used to hand over the tundish like a mobile to the crane (Figure 7).

The crane transported the sandwich to the EAF. After opening the furnace roof, the tundish sandwich was lowered to the melt. Due to the heat of the melt, the steel rods fused, and the sandwich went into the melt (Figure 8). This process was repeated four times, resulting in the construction of four sandwich forms which were charged into the EAF four times in different heats. During the tests, standard

Parameter	Unit	LFS1	LFS2	LFS3
Al_2O_3	wt.-%	4.82	6.64	17.19
BaO	wt.-%	< 0.020	0.026	< 0.020
CaO	wt.-%	50.6	38.8	38.67
CO_2	wt.-%	1.8	3.2	0.72
Cr_2O_3	wt.-%	0.36	1.03	0.12
CuO	wt.-%	< 0.020	0.065	< 0.01
FeO	wt.-%	5.09	11.7	2.36
K_2O	wt.-%	< 0.020	0.023	0.12
MgO	wt.-%	7.1	10.8	13.28
MnO	wt.-%	1.24	1.78	0.44
Na_2O	wt.-%	< 0.020	< 0.020	0.04
P_2O_5	wt.-%	0.053	0.073	0.03
SO_4	wt.-%	2.24	1.11	1.86
SiO_2	wt.-%	19.1	19.5	19.21
TiO_2	wt.-%	0.32	0.25	0.25
V_2O_5	wt.-%	0.027	0.036	0.02
ZnO	wt.-%	0.033	0.038	0.05
C/S*		2.65	1.99	2.01
C+M/S+A**		2.41	1.90	1.43

** Basicity: CaO %/SiO_2 %, ** Basicity: (CaO %+MgO %)/(SiO_2 %+Al_2O_3 %)*

Table 1: Chemical composition of LF slag used for disintegration experiments

Mineral	Formel	LFS1	LFS2	LFS3
Calcio-Olivine	Ca_2SiO_4	20	15	
Larnite	Ca_2SiO_4	35		1
Merwinite	$Ca_3MgSi_2O_8$		35	49
Cuspidine	Ca4Si2O7F2		20	
Jasmundite	$Ca_{20.68}Mg_{1.32}(SiO_4)_8O_4S_2$	5		
Gehlenite	$Ca_2Mg_{0.25}Al_{1.5}Si_{1.25}O_7$		5	35
Tri-Calcium-Aluminate	$Ca_3Al_2O_6$	< 5		
Mayenite	$Ca_{12}Al_{14}O_{33}$			
Bredigite	$Ca_{1.7}Mg_{0.3}SiO_4$	15		
Fluorite	CaF_2	< 5		
Wuestite	FeO_x	< 5	< 5	
Free lime	CaO			
Portlandite	$Ca(OH)_2$	< 5		
Calcite	$CaCO_3$		5	
Periclase	MgO	5	10	15
Brucite	$Mg(OH)_2$	< 5	5	
Sjogrenite	$Mg_6Fe_2(OH)_{16}CO_3$ x $4,5H_2O$		< 5	

Table 2: Mineral composition of LF slag used for disintegration experiments

procedures were followed for the EAF without any changes to the additions. This means that the sandwich structure was added in addition to the lime/dolomite addition.

Chemical composition

The chemical composition of the LF slag samples was determined according to DIN EN ISO 12677. Samples were fused and measured subsequently by XRF.

Mineral composition

For the mineralogical analysis, samples were dried in a vacuum, milled, and sieved at 63 µm. X-ray diffraction was performed on the < 63 µm fraction with Cu k-alpha1 radiation in the range 5 to 75 °2-theta (PANalytical, type X'Pert pro). Qualitative analysis was done using pdf-2; quantification by Reference-Intensity-Ratios. The analytical error is estimated at 5%–10%.

Leaching analysis

The leaching test described in this report is based on EN 12457-4 for a 1:10 slag to water ratio as well as DIN 19529 for a 1:2 slag to water ratio. The grain size of slag used was 8–11 mm. The resulting leachate was analysed with ICP-OES (Varian Vista MPX and Spectro Ciros, with an analytical error of 3%).

LABORATORY EXPERIMENTS

Results of laboratory LF slag disintegration temperature tests

The chemical and mineral properties of the slag samples LFS1, LFS2 and LF3 used in disintegration temperature tests are presented in Table 1 and Table 2, respectively.

The LFS1 slag started to disintegrate at about 195°C (Figure 9), the LFS2 slag started to disintegrate at about 135°C (Figure 10), and the LFS3 slag started to disintegrate at about 170°C (Figure 11).

Parameter	Unit	Ref 1	Ref 2	Ref 3	Ref 4	Av	Trial 1	Trial 2	Trial 3	Trial 4	Av
pH		11.3	11.4	11.4	11.3	11.4	11.6	11.5	11.5	12.0	11.7
LF	µS/cm	600	654	624	615	623	1.210	1.104	910	2.390	910
Ca	mg/l	43.43	44.74	41.39	46.79	44.09	125	110	72.4	191	125
Cr	mg/l	< 0.002	0.003	0.003	< 0.002	0.003	0.007	0.006	0.002	0.019	0.009
Mo	mg/l	0.083	0.105	0.074	0.102	0.091	0.190	0.216	0.012	0.030	0.112
V	mg/l	0.174	0.065	0.069	0.135	0.111	0.014	0.017	0.044	< 0.002	0.025
F	mg/l	1.5	1.4	1.4	2.0	1.6	2.1	2.0	2.4	1.2	1.9

Table 3: Concentrations of the leachates of 4 reference samples and the 4 ECOSLAG trials

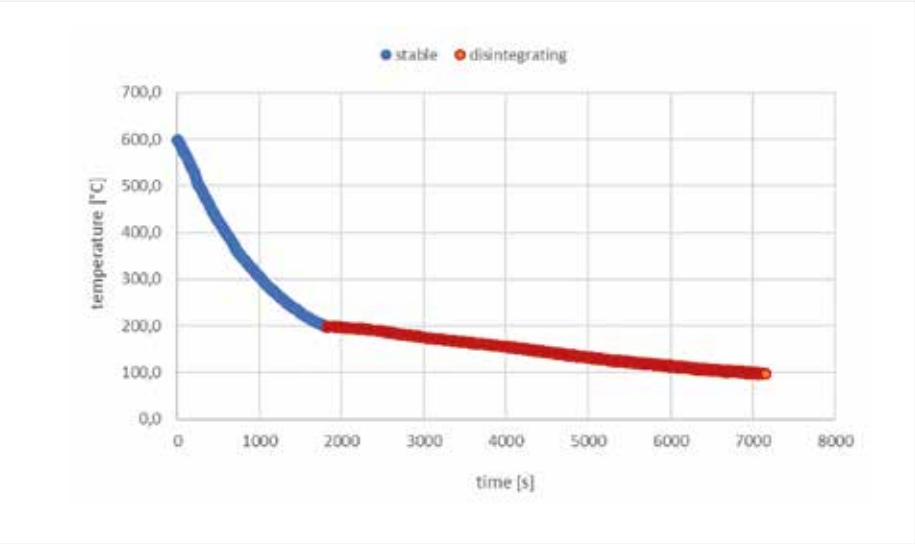

Figure 9: Temperature reading of the LFS1 slag sample during cooling (blue before signs of disintegration and orange after the slag started to disintegrate)

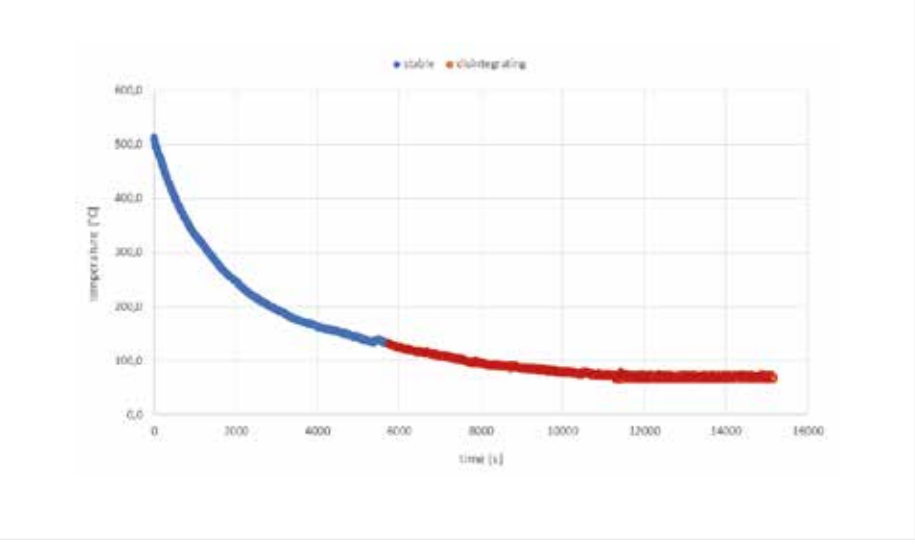

Figure 10: Temperature reading of the LFS2 slag sample during cooling (blue before signs of disintegration and orange after the slag started to disintegrate)

With respect to this information, the LF slag in sandwich tests would be charged to the EAF before it cools down to about 200°C but keeping in mind that the exterior of the slag will cool down faster than the inside.

Industrial trials of the sandwich concept

The 4 sandwich slag/metal structures were charged into the EAF without major issues. However, further trials would have to take factors into consideration. In the ECOSLAG project, only 4 industrial trials were conducted as the sandwich concept was investigated. No changes were made to the standard EAF process while the sandwich was charged. This means that the LF slag was added in addition to the regular amount of lime/dolomite that was added. Four sandwich additions into the EAF are not enough to understand the exact effect of adding LF slag to the EAF. For example, continuous tests over a few months would allow the steelwork to calculate by how much it can reduce lime addition because this would be substituted with LF slag to achieve their required steel grade.

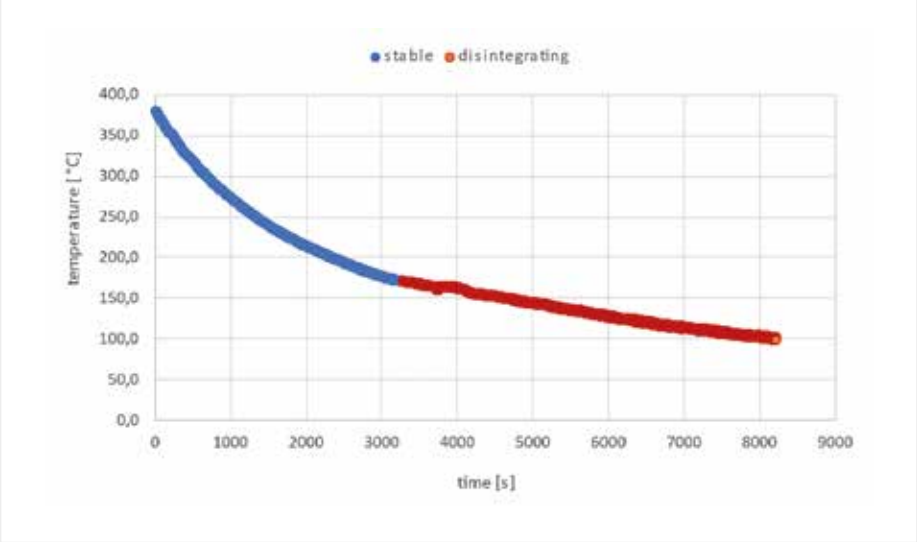

Figure 11: Temperature reading of the LFS3 slag sample during cooling (blue before signs of disintegration and orange after the slag started to disintegrate)

Temperature	Heat capacity LF slag	Heat capacity steel
473 K	82.1 kWh/t	57.8 kWh/t
1273 K	374.1 kWh/t	206.7 kWh/t
1823 K	587.8 kWh/t	414.1 kWh/t

Table 4: Heat capacity of LF slag and steel

EAF slag quality

The EAF slag of each heat, where a LF slag sandwich was charged to the EAF, was analysed in terms of leaching to assess the impact on environmental compatibility. The lime addition of the heat was not reduced due to the risk of a too low CaO content in the slag and therefore was not usable crude steel. Four reference samples were also taken with the same scrap input, to have a valid comparison (Table 3).

This resulted in an increase in the lime content, which can be seen in the increase in Ca concentration in the leachate. A higher Ca concentration often leads to decreased V leaching, which was also observed during these tests. There was no negative impact from charging the sandwich of LF slag and steel to the EAF. The higher lime content leads to a slightly improved slag quality, and additionally by implementing this technique in operational practice, the addition of virgin lime would be decreased to save natural resources, such as CO_2 and energy for melting of the lime.

Potential energy recovery from hot LF slag sandwich charging into an EAF

Recycling of LF slag into an EAF to recover the energy can take place in a temperature range from 1,550°C to 200°C. The best case is when the slag is liquid at 1,550°C, because this is the typical tapping temperature of the slag. The worst case is around 200°C (473 K), because below this temperature the slag starts to disintegrate, making transportation and charging to the EAF without high dust emissions impossible. A temperature of 1,000°C (1273 K) is the realistic case and was defined as the aim of the project, where the slag is definitely solidified and good to handle but still at a high temperature.

Based on this temperature and the average LF slag composition, the following heat capacities of slag and steel, simplified by using the heat capacity of iron, were calculated (Table 4).

Assuming production of around 30,000 t of LF slag per year and additionally around 15,000 t of remaining steel in the LF slag (actual ratio of 2:1), the heat potentials at these different temperatures are:

473 K:	3,330 MWh/a
1273 K:	14,324 MWh/a
1823 K:	23,846 MWh/a

By recharging all the material into the EAF with the sandwich concept developed in the ECOSLAG project, there is a potential of recovering 14,324 MWh per year. Recharging of liquid LF slag would nearly double the energy recovered, but this is not possible in most of the steelworks due to the logistics of transporting LF slag.

Energy consumption of EAF during trials

Due to the small number of trials and the large variation in electricity consumption of the EAF, it was not possible to see any real electricity changes due to the charging of the hot LF slag sandwiches (see Figure 12 and Figure 13). To detect possible electricity savings,

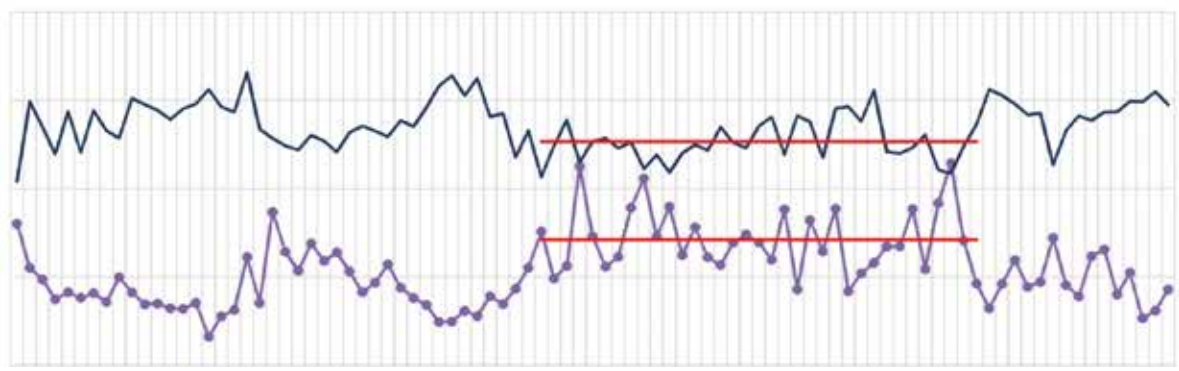

Figure 12: Energy input/ for liquid steel yield (how much material comes out compared with input); the red line designates the period during test trials

Figure 13: Energy input/ for liquid steel yield (black line/orange arrow = test charge)

continuous charging of LF slag would have to take place over a long period of time (e.g. a month of continuous trials), so that the variations could be clearly attributed to the heat from the LF slag. However, Figure 12 and Figure 13 show that no extra energy was used in order to melt the LF slag sandwiches.

Environmental outlook

The recycling of LF slag into an EAF will result in environmental benefits with respect to a decrease or substitution of natural lime as slag former in the EAF, a decrease in landfilled LF slag, a decrease in dust emission during handling of LF slag and a decrease in water consumption and pollution for LF slag handling. If the tests were to be carried out over a longer period of time (1–6 months), it would be possible to see how much electricity consumption would be saved due to the input of the hot LF slag and steel. Even a small decrease in electricity consumption would result in energy savings that the steelwork needs to run the EAF.

The decrease in the input of natural lime into the EAF, which is used as a slag former, would be possible with the substitution of LF slag, which would save natural resources. In these trials, the steelwork did not decrease the amount of lime that was added into the EAF when the hot LF slag was added. In the future, continuous addition of LF slag will enable calculation and the gaining of experience in practice.

In addition, even partial reutilization of LF slag directly in an EAF to substitute lime (natural resource) will decrease the amount of slag that needs to be landfilled, which will make steelworks more sustainable. Today, handling of disin-

tegrated LF slag means dust emissions and water consumption resulting in pollution that could be completely avoided.

SUMMARY

An advanced solidification system for LF slag was designed to keep the temperature of the solidified LF slag above the starting temperature of dicalcium silicate (C2S) disintegration. This way, C2S disintegration, which results in high dust emissions, was prevented and the maximum practical potential of thermal energy is available for heat recovery. After solidification of the outer surface, the hot LF slag sandwich was charged/recycled to the EAF. In operational practice, the addition of LF slag can substitute conventional lime in the process. The charging of the hot LF slag as a lime substitute plus hot steel is the most efficient way to recover heat from the slag. Thermal energy is directly fed back into the steelmaking process without energy losses at, e.g., the heat exchanger.

The ECOSLAG project showed that recycling of LF slag into an EAF is possible by using the sandwich concept, even with the restrictive logistical situation faced by some steelworks, but further research would be needed in order to understand how much lime can be substituted by LF slag without changing current steel production. Based on the economic evaluation, implementing this technique in operational practice would be beneficial. However, the security risks from a brake of the sandwich must be minimised. The plan is to identify possible devices to minimise this risk with a plan to bring this technique in operational practice.

ACKNOWLEDGEMENT

This research was funded by the European Union's Research Fund for Coal and Steel research programme under grant agreement no. 800762 <<<

LITERATURE

[1] Best Available Techniques (BAT) Reference Document for Iron and Steel production, Industrial Emissions Directive 2010/75/EU, (Integrated Pollution Prevention and Control) EUROPEAN COMMISSION JOINT RESEARCH CENTRE, Institute for Prospective Technological Studies Sustainable Production and Consumption Unit, European IPPC Bureau, 2013, p. 429
[2] EUROFER Association, eurofer.eu
[3] European Commission, Directorate-General for Research and Innovation, Kuehn, M., Drissen, P., Cores, A., Efficient utilisation of raw materials used in secondary steelmaking as flux in steelmaking furnaces, Publications Office, 2005
[4] European Commission, Directorate-General for Research and Innovation, Colla, V., Klung, J., Bardella, S., et al., Environmental impact evaluation and effective management of resources in the EAF steelmaking (EIRES) : final report, Publications Office, 2018, https://data.europa.eu/doi/10.2777/86516
[5] European Commission, Directorate-General for Research and Innovation, Kozariszczuk, M., Wendler, B., Cirilli, F., et al., Control of slag quality for utilisation in the construction industry (SLACON) : final report, Publications Office, 2017, https://data.europa.eu/doi/10.2777/84385
[6] European Commission, Directorate-General for Research and Innovation, Zetterholm, J., Heintz, I., Wedholm, A., et al., Efficient use of resources in steel plant through process integration (Reffiplant): final report, Publications Office, 2017, https://data.europa.eu/doi/10.2777/052290
[7] European Commission, Directorate-General for Research and Innovation, Kuehn, M., Drissen, P., Cores, A., Efficient utilisation of raw materials used in secondary steelmaking as flux in steelmaking furnaces, Publications Office, 2005
[8] European Commission, Directorate-General for Research and Innovation, Colla, V., Klung, J., Bardella, S., et al., Environmental impact evaluation and effective management of resources in the EAF steelmaking (EIRES): final report, Publications Office, 2018

FIRST RESULTS FROM THE REPHOR JOINT PROJECT R-RHENANIA

Dr. sc. agr. H.-P. König
(FEhS — Building Materials Institute)

Dr. U. Arnold; PD Dr. J. Burkhardt; K. Leers
(University of Bonn, INRES – Institute of Crop Science and Resource Conservation, Division Plant Nutrition, Bonn)

INTRODUCTION

Phosphorus in the form of phosphate is an indispensable nutrient for plants, animals and humans. Animals and humans absorb the phosphate they need through feed and food. In agricultural ecosystems, the availability of this nutritive element is very limited and it must be added through fertilisation regularly. While phosphate excreted by farm animals is reused for fertilisation in the form of manure or slurry, phosphate from human nutrition is lost to agricultural use. After it has been excreted, phosphate is precipitated in sewage treatment plants and incinerated together with sewage sludge.

In agricultural fertilisation, it is common practice to replace nutrient losses with mineral fertilisers. Mineral phosphate fertilisers are extracted from natural deposits. However, these deposits are finite and are also mainly located in non-EU countries. In order to conserve these deposits and reduce the dependence on imports, the legislator has obliged the operators of wastewater treatment plants to recover phosphate from wastewater treatment in the future.

The aim of the R-Rhenania project is to process the poorly plant-available phosphate contained in sewage sludge ashes into a better plant-available modified Rhenania phosphate (Ca-Na-silicophosphate). Another goal of the treatment process is the reduction of heavy metals contained in sewage sludge ashes. For these purposes, the sewage sludge ash is heated to over 900°C in a rotary kiln (AshDec process) with the addition of Na-containing additives [1]. The experimental fertilisers (AshDec) required for the plant trials were produced in a laboratory plant. In the second phase of the project, a pilot plant will be built and the fertilisers produced in it will then be compared again with the products from the laboratory plant.

MATERIALS AND METHODS

In order to test the effectiveness of the fertilisers produced, both field trials by the Bavarian State Research Center for Agriculture (LfL) at three sites in Bavaria and container trials at Bonn University with soil material from the field trial sites and a lawn substrate were carried out as part of the project. The analysis of the soil and plant material from the container trials was carried out at the FEhS Institute. The first results of the container trial with the lawn substrate are presented below.

The containers were sown with wheat and fertilised with the experimental fertilisers at two P fertilisation levels (0.2 g fertiliser-P per container and 0.4 g fertiliser-P per container, labelled 1 and 2 respectively in the following figures) based on the total P content of the respective fertiliser (Table 1). The fertiliser produced from sewage sludge ash in the project (AshDec) was tested against a control without P fertilisation (zero P), untreated sewage sludge ash (SSA), rock phosphate (RP), triple superphosphate (TSP) and a combination of triple superphosphate and water-soluble sodium metasilicate (Si). The experimental elements with TSP and sodium metasilicate (Si-1 and Si-2) were designed to compare the uptake of silica from the AshDec and sewage sludge

	sewage sludge ash	AshDec	Rock phosphate	Triple super-phosphate
P_2O_5–total content	21.8%	20.1%	27.4%	49.3%
P_2O_5–citric acid soluble	10.9%	17.4%	ND	ND
P_2O_5–neutral ammoncit. sol.	9.7%	18.5%	6.1%	46.8%
P_2O_5–water soluble	0.01%	0.53%	0.1%	43.6%

Table 1: Phosphate contents and solubilities of the experimental fertilisers

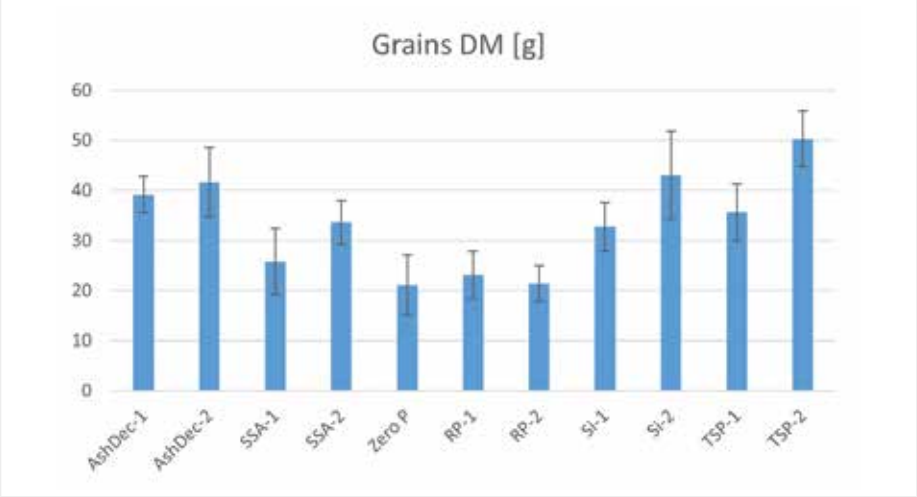

Figure 1: Grain dry matter yield per container on lawn substrate. Experimental results of the project partner Bonn University. Error bars represent the standard deviation

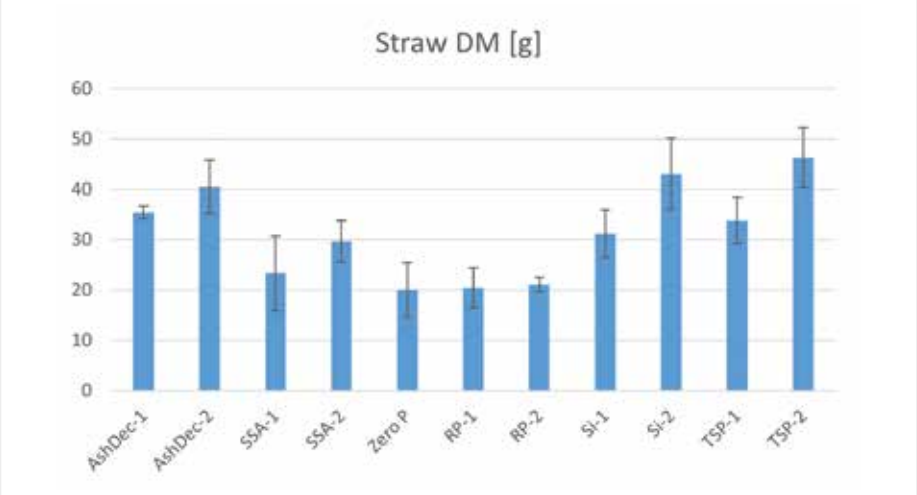

Figure 2: Straw dry matter yield per container on lawn substrate. Experimental results of the project partner Bonn University. Error bars represent the standard deviation

ash material and to test the effect on nutrient status [2, 3, 4]. In addition, the effect of water-soluble silica on heavy metal uptake into the plant will also be tested, as there are various indications in the literature that it suppresses arsenic or cadmium, for example [5, 6]. All other nutrients were fertilised at the levels required for plant growth, including in the zero P control. The container trial was set up in five replicates. After the end of the trial, the wheat was harvested, i.e., the yield of grain and straw was determined, and analysed for plant nutrient content and heavy metal content. The analysis of the soil samples and the evaluation of the data are still ongoing.

FIRST RESULTS OF THE POT TRIAL WITH LAWN SUBSTRATE AND DISCUSSION

Thermal treatment of the sewage sludge ash in a rotary kiln significantly improved the phosphate solubility in the experimental fertiliser AshDec (Table 1). The citric acid soluble phosphate content increased from 10.9% in the sewage sludge ash to 17.4% P_2O_5 in AshDec. The neutral ammonium citrate solubility improved even more markedly from 9.7% to 18.5% P_2O_5. With this solubility improvement, plant availability also improved significantly.

As expected, grain and straw yield reacted positively to the P fertilisation (cf. Figure 1 and 2), although the difference between the two fertilisation levels was not particularly large and probably cannot be statistically confirmed. The yield of the sewage sludge ash treatments was below the yield level of the AshDec and triple superphosphate treatments, i.e., the plant availability of the phosphate contained therein is lower than that of the AshDec material. In contrast, the two rock phosphate treatments showed no yield effect. Rock phosphates that are not processed before application initially

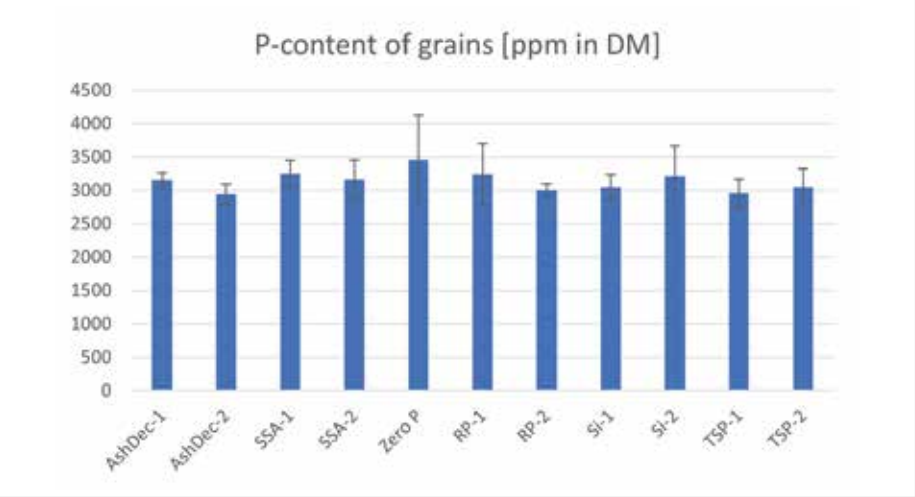

Figure 3: Phosphorus content in grain dry matter. Error bars represent the standard deviation

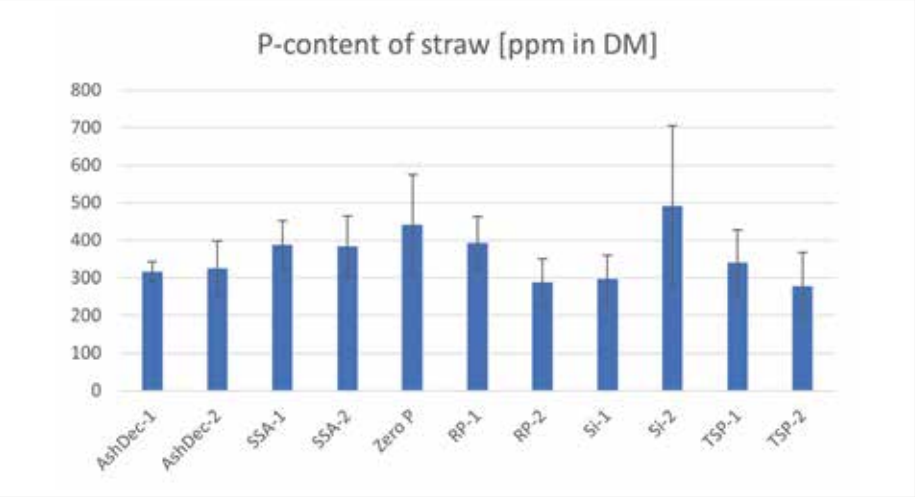

Figure 4: Phosphorus content in dry straw mass. Error bars represent the standard deviation

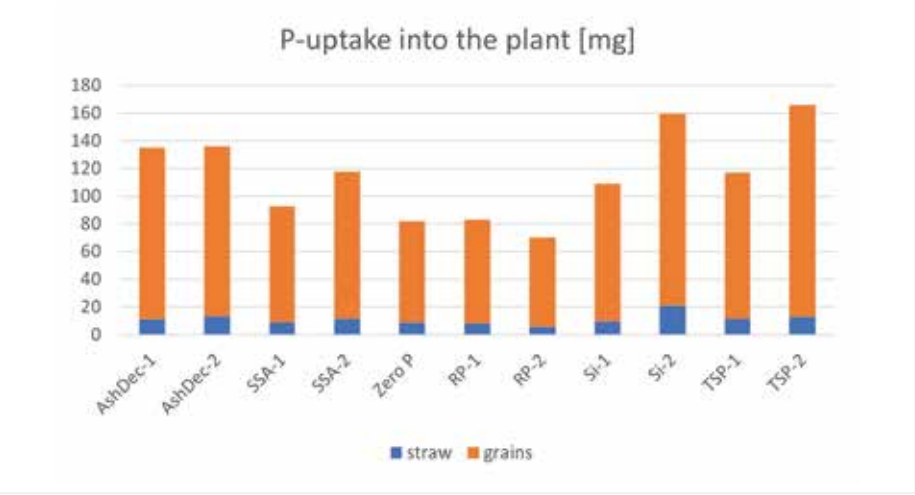

Figure 5: Absolute P uptake per container in grain and straw, calculated from dry mass yield and P contents in the plant material

have no fertilisation effect and at most have a long-term effect, so that they also did not differ from the zero P trial member. From the yield data, it can be concluded that the AshDec fertiliser is approximately comparable with the triple superphosphate trial members in terms of plant availability.

The P content in grain and straw did not show a particularly clear picture. While the P content in the grains showed almost no difference between the trial members, if one disregards the zero P trial member (cf. Figure 3), one could deduce from the results of the P content in the straw that with increasing biomass there is a dilution of the P content (cf. Figure 4). For example, the trial elements of the high fertilisation level have the same or even a slightly lower P content in the straw. Only in the straw of treatment Si-2 was a higher P content measured than in all other trial members. However, the highest standard deviation also occurred here.

By calculating the P uptake from yield and P content in the biomass, the absolute amount of P taken up can be compared between treatments (Figure 5). Here, it can be seen that the zero P and the two rock phosphate fertilisation levels had taken up the least P into the biomass. For sewage sludge ash, triple superphosphate and triple superphosphate with sodium metasilicate, P uptake was, as expected, graded according to the fertilisation level. An improvement in P uptake through the addition of sodium metasilicate cannot be deduced from the results. The two AshDec fertilisation levels showed no difference in P uptake.

CONCLUSION

The expected improvement in plant availability of the processed sewage sludge ash to AshDec could be shown both by laboratory analyses on the experimental fertiliser AshDec and on the results of the vessel trial. From a plant cultivation point of view, and also with regard to the accumulation of poorly soluble phosphates in soil, the processing of sewage sludge ash makes sense in any case in order to use the resource phosphate more efficiently.

The addition of water-soluble sodium metasilicate showed no effect on the P content for the time being. The evaluation of the trace element data will show whether there were any reducing effects and whether such effects can also be caused by silicic acid from the AshDec.

The existing data material will be further analysed, in particular to examine the effect of silicon on the uptake of heavy metals in more detail. In the second phase of the project, the experimental approaches will be refined on the basis of these results and any new questions that arise will be addressed in a targeted manner.

ACKNOWLEDGEMENT

The RePhoR - joint project R-Rhenania: Modified Rhenania Phosphate from Sewage Sludge Ash for Bavaria, sub-project 7, funding code 02WPR1547G, is funded by the Federal Ministry of Education and Research/PTKA. We would like to express our sincere thanks for the funding. <<<

LITERATURE

[1] Adam, Chr.: Phosphatdüngemittel aus Klärschlammaschen. Technik in Bayern, 03/2020
[2] Eurich-Menden, B.: Der Einfluss silikatischer Kalke auf die Phosphorverfügbarkeit und Aggre-gatstabilität landwirtschaftlich genutzter Böden unter besonderer Berücksichtigung der löslichen Kieselsäure. Boden und Landschaft 7, Justus-Liebig-Universität Gießen, 1996
[3] Rex, M., H. Munk: Düngung mit silikatischen Kalken und Einfluss auf Ertrag sowie SiO_2-Gehalte in Boden und Pflanze; VDLUFA-Schriftenreihe 28, Seiten 389-402, Kongressband 1988
[4] Greger, M., T. Landberg, M. Vaculík, M.: Silicon influences soil availability and accu-mulation of mineral nutrients in various plant species; Plants 7, 41, 2018
[5] Tripathi, P., Tripathi, R.D., Singh, R.P., Dwivedi, S., Goutam, D., Shri, M., Trivedi, P.K., Chakrabarty, D.: Silicon mediates arsenic tolerance in rice (oryza sativa l.) through lowering of arsenic uptake and improved antioxidant defence system. Ecological engineering (2013), 52, 96-103
[6] Treder, W., Cieslinski, G.: Effect of silicon application on cadmium uptake and distribution in strawberry plants grown on contaminated soils. Journal of plant nutrition 28, 917-929, 2005

PRODUCTION AND USE OF FERROUS SLAG IN 2021

Dr.-Ing. Th. Merkel
(FEhS — Building Materials Institute)

Ferrous slag (blast furnace slag and steel furnace slag) has for decades been an established product in construction and fertilising. The ratio of use exceeds 90% of the production, so the use of slag is a best practice example of conservation of natural resources.

GERMANY

Data concerning production and use in Germany in 2021 are given in Tables 1 (blast furnace slag) and 2 (steel furnace slag). For comparison, the data for 2020 are shown also.

Production	2021	2020
Granulated BFS	**6.90**	5.80
Air-cooled BFS	**0.72**	0.61
Sum	**7.62**	6.41
From interim storage	**0.87**	0.91
Total	**8.49**	7.32

Use	2021	2020
ABS for aggregates	**0.29**	0.27
ABS for aggregate mixtures	**0.59**	0.48
GBS for cement production	**7.41**	6.42
GBS for other purposes	**0.10**	0.08
Intra-industrial consumption	**0.10**	0.07
Total	**8.49**	**7.32**

Tables 1: Production and use of blast furnace slag in Germany in 2021/2020 (in million tonnes)

Production	2021	2020
Slag from oxygen steel making	**2.82**	2.53
Slag from electric arc steel making	**1.58**	1.46
Others (SecMS etc.)	**0.58**	0.46
Sum	**4.98**	4.45
From interim storage		0.01
Total	**4.98**	**4.46**

Use	2021	2020
Metallurgical use	**0.51**	0.61
Fertiliser	**0.40**	0.43
Construction material	**2.56**	2.66
Others	**0.31**	0.21
Sum	**3.78**	3.91
Final deposit	**0.44**	0.55
To interim storage	**0.76**	
Total	**4.98**	4.46

Tables 2: Production and use of steel furnace slag in Germany in 2021/2020 (in million tonnes)

In 2021, total crude steel production in Germany was 40.1 million tonnes [1]. After a decrease to 35.7 million tonnes in 2020, caused in particular by the pandemic situation, steel production roughly reached the level of 2019 again. The production of by-products also correspondingly increased: in 2021, 12.6 million tonnes of ferrous slag were produced after 10.9 million tonnes in 2020. Additionally, 0.1 million tonnes of slag were recovered from interim storage.

As before, the ratio of granulation is about 90% of blast furnace slag (BFS) and the proportion of granulated BFS (GBS) used for cement production was 97%. This clearly highlights how important the production of CEM-II/S cements and CEM-III cements is for the cement industry. These cement types provide an important contribution to CO_2 saving in cement production. Air-cooled blast furnace slag (ABS) was mainly processed to aggregate mixtures for road construction. But at a progressive rate, ABS is processed to aggregates for asphalt mixes and concrete.

The total production of steel furnace slag (SFS) in 2021 was 4.9 million tonnes, following 4.5 million tonnes in 2020. Even if the production increased, the utilisation decreased. Perhaps there was

a lack of big construction sites, possibly caused by the ongoing pandemic situation. But as before, the market for construction products is most important for SFS products (2.6 million tonnes, 2020 2.7 million tonnes). A volume of 0.4 million tonnes was used as fertiliser and 0.5 million tonnes was used to provide lime and iron for metallurgical processes.

In total, in 2020 in Germany 12.3 million tonnes of slag products were sold, an impressive number compared with the production of 12.6 million tonnes.

EUROPE

The European slag association, EUROSLAG, regularly asks its members for European slag data. Preliminary figures for 2021 are given in Tables 3 (blast furnace slag) and 4 (steel furnace slag). However, these figures must be qualified as it has not yet been possible to obtain a satisfactory number of responses.

Based on the hot metal and crude steel production provided by Worldsteel [1], a respectable estimation of BFS production and SFS production can be made. This results in about 25 million tonnes of BFS and 17 million tonnes of SFS produced in the EU-27 countries + UK during the year 2021. The reported data provided in Tables 3 and 4 represent about 71% of the BFS and 74% of the SFS figures. These are roughly the percentages obtained for the year 2020, so a comparison between the years 2021 and 2020 is generally possible, even if the reporting countries are not exactly the same.

Comparison of the production figures reveals an increase in production especially for BFS, as reported above for Germany. A difference seems to exist in SFS production, as the estimated sum is roughly the same as in the previous year.

Comparing the percentages for BFS with those reported from Germany reveals the figures are quite close together: about 90% of the blast furnace slag is granulated and subsequently 90% of it is used for cement production. The second largest amount is used as aggregate or aggregate mix for construction purposes. Only a small amount is used for other purposes such as fertilising and glass production.

About 80% of the SFS produced is used for construction purposes, for example for roads, dams or hydraulic structures. About 15% is used for metallurgical purposes, 5% as fertiliser and a small percentage for other uses. 10% of the SFS produced went to interim storage to be utilised later, and 14% was ultimately deposited. Altogether the (reported) use is close to the (reported) production not only in Germany but also throughout Europe. Steel producing companies together with processing and marketing companies do their best to enable a circular economy. <<<

Production	2021	2020
Granulated BFS	**15.6**	14.3
Air-cooled BFS	**2.3**	1.9
Sum	**17.9**	16.2
From interim storage	**2.0**	1.7
Total	**19.9**	17.9

Use	2021	2020
Cement production and concrete additives	**16.5**	14.6
Road construction	**3.1**	2.8
Others	**0.3**	0.3
Final deposit		0.2
Total	**19.9**	17.9

Production and use of blast furnace slag in Europe in 2021/2020 (in million tonnes)

Production	2021	2020
Slag from oxygen steel making	**6.8**	6.0
Slag from electric arc steel making	**4.0**	3.9
Others (SecMS etc.)	**1.7**	1.4
Total	**12.5**	11.3

Use	2021	2020
Metallurgical use	**1.4**	1.1
Fertiliser	**0.4**	0.6
Construction material	**7.6**	8.0
Others	**0.1**	0.6
Sum	**9.5**	10.3
Final deposit	**1.7**	1.0
To interim storage	**1.3**	< 0.1
Total	**12.5**	11.3

Tables 4: Production and use of steel furnace slag in Europe in 2021/2020 (in million tonnes)

LITERATURE

[1] Worldsteel Association: 2022 World Steel in Figures. Brussels, 2022

"ACTISLAG" – NEW ACTIVATION ROUTES FOR EARLY STRENGTH DEVELOPMENT OF GRANULATED BLAST FURNACE SLAG

Dr.-Ing. Andreas Ehrenberg
(FEhS — Building Materials Institute)

Figure 1: "ActiSlag" project partners

INTRODUCTION

From 2017 to 2021, the RFCS project 749809 „New activation routes for early strength development of granulated blast furnace slag (ActiSlag)" was implemented. The project coordinator was ArcelorMittal Maizières Research (Metz). Besides the FEhS Institute, the additional partners were the Centre National de la Recherche Scientifique (CEMHTI - Conditions Extrêmes et Matériaux: Haute Température et Irradiation, Orleans), the University Paul Sabatier (LMDC - Laboratoire Matériaux et Durabilité des Constructions, Toulouse), the Technical University of Clausthal (TUC), the Institute for Non-Metallic Materials, Clausthal-Zellerfeld, and the GGBS producer ECOCEM Materials Ltd., Dublin (Figure 1).

This publication is focused on activities relating to chemical slag properties, glass structure and reactivity. A detailed discussion of all comprehensive results provided by all project partners is impossible. Thus, it should be permitted to refer to the different publications already published by the partners, [1, 2, 3, 4, 5, 6].

Moreover, the results have been presented in shortened form at numerous conferences and seminars [7, 8, 9, 10, 11, 12, 13, 14].

PROJECT TARGETS

The main objectives of the very ambitious project were to understand more precisely which chemical and thermal parameters influence granulated blast furnace slag (GBS) quality and the performance of GBS in cement and concrete. Accordingly, the micro and nanostructure of the amorphous phase, some minor chemical elements besides the major oxides (CaO, SiO_2, Al_2O_3, MgO), and the mechanism of early age hydration have been investigated. The main target was to improve the short-term performance and the performance of cements with high GBS content. To achieve this target, both the „upstream activation" measurements of the liquid blast furnace slag (= chemical and thermal modifications of the glass structure) during the melting and granulation processes and the „downstream activation" measurements of the solid slag, such as combinations with chemical activators (e.g., NaCl, $CaCl_2$, Na_2SO_4, NaSCN and triethanolamine) have been tested. With respect to the practice, a „second generation GBS" should be developed. Thus, a blast furnace cement CEM III/B with 80 wt.-% GBS should show a similar (early) strength performance as a composite cement CEM II with only 20 wt.-% GBS (18–24 MPa after 2 days).

TASKS OF THE DIFFERENT PROJECT PARTNERS

Each partner had specific work topics within the 6 working packages of the project. ArcelorMittal Maizières Research coordinated the project and many lab-scale GBS samples were produced in small quantities with varying slag chemistry and granulation conditions. Moreover, a test on an industrial scale was organised (increase in Al_2O_3 content) and ecological aspects were evaluated. Based on its database, the FEhS selected 16 different industrial GBS which were characterised in terms of chemical, physical and cementitious properties according to the usual standards. Moreover, several lab-scale modified GBS were produced in larger quantities. The TUC mainly characterised the thermal history of the granulated slags by adopting the so-called „hyperquenching-annealing-calorimetry" approach based on Differential Scanning Calorimetry (DSC) analyses of glassy GBS [15, 16, 17, 18]. In addition, simultaneous thermal analysis coupled with mass spectrometry (STA-MS) were done combining information from thermogravimetric data, differential thermal analysis (DTA) data and data on volatile constituents. The CEMHTI characterised mainly the atomic Si, Al and Na coordination both in industrial and lab-scale GBS glasses and in model glasses and hydration products by means of ^{29}Si, ^{27}Al and ^{23}Na magic angle spinning (MAS) nuclear magnetic resonance (NMR) spectroscopy. For some samples, scanning electron microscopy (SEM)/energy-dispersive X-ray spectroscopy (EDS) and transmission electron microscopy (TEM) analyses were also conducted to evaluate the homogeneity of GBS glass. The LMDC optimised a fast test procedure to evaluate the reactivity of GBS based on the RILEM R3 heat of hydration test procedu-

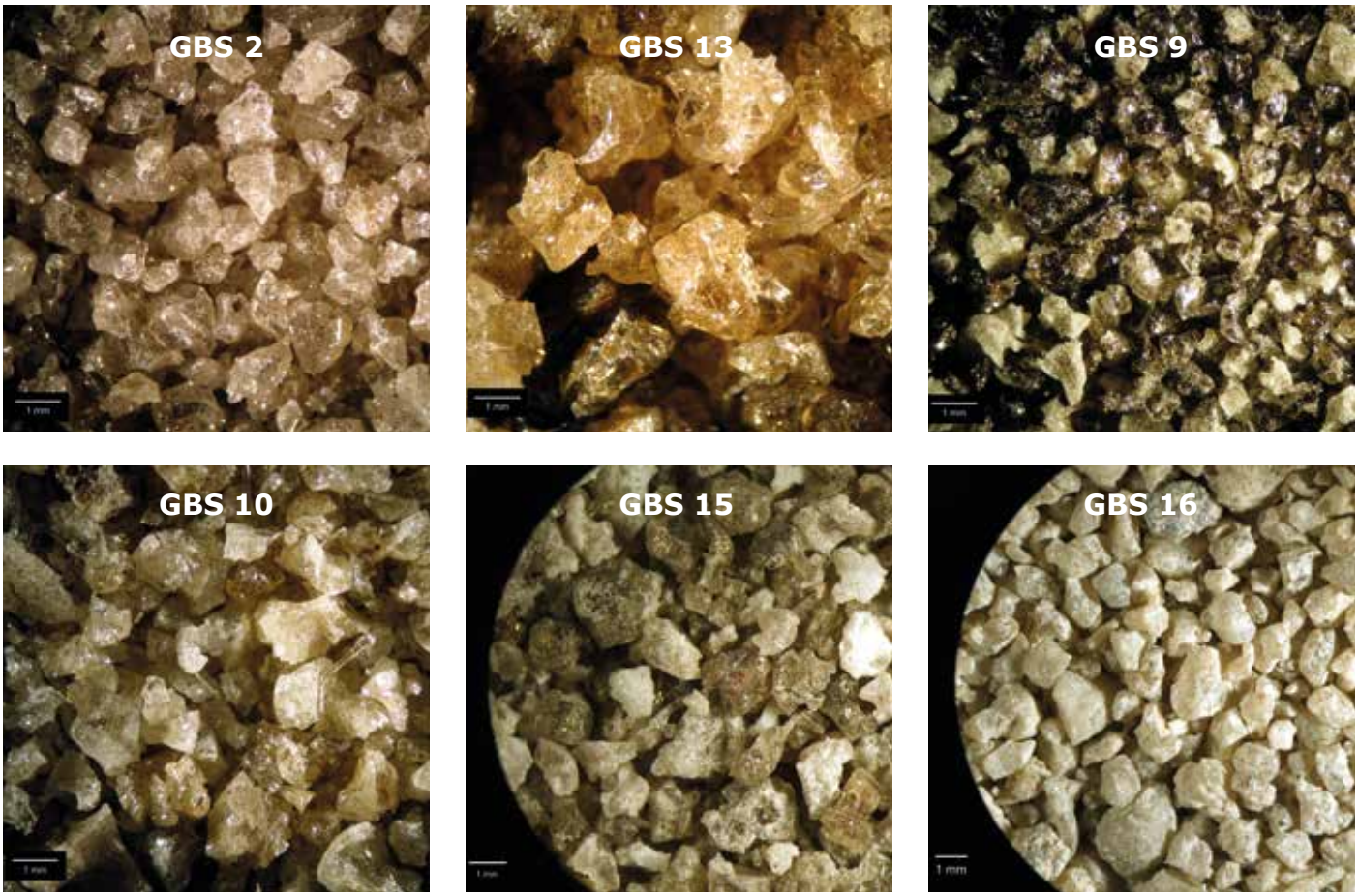

Figure 2: 6 of the 16 industrial GBS (original, reflected light microscopy)

re [19]. Moreover, a lot of hydration and slag glass dissolution tests were carried out. In addition, besides SEM and TEM, complex micro-X-ray absorption near edge structure (XANES) and synchrotron X-ray microtomography (XMT) analyses were also conducted. In particular, the in situ observation of samples during the early hydration time was of great interest. ECOCEM supported the work of the LMDC, in particular regarding the development of optimised building materials, such as by „downstream activation".

CHARACTERISATION OF INDUSTRIAL GBS

Based on the GBS database of the FEhS and proposals by ArcelorMittal, 14 industrial GBS from Europe (GBS 1–14) and two industrial GBS from India (GBS 15) and the USA (GBS 16) were selected. Figure 2 shows 6 of the 16 samples. The FEhS analysed chemical composition (main and minor constituents and heavy metals), glass content, physical properties (true, apparent, bulk densities, grain porosity, grading curve, Vickers hardness), grindability and cementitious properties. The samples covered a wide range of chemical compositions of GBS (Table 1). The minimum glass content value was 96.6 vol.-%. The glass contents confirm that very high values are achieved in most of today's granulation facilities. Figure 3 shows six examples of GBS (crushed, fractions of 40–63 µm) investigated by transition light microscopy to measure the glass content [20].

It is well known that GBS reactivity depends on several factors, such as chemical composition, glass content and thermal history [21]. Because most GBS are more or less glassy, the stability of the glass in alkaline solutions is an essential topic. Many glass properties can be explained with the SiO_4^{4-} network theory of Zachariasen and Warren [22]. SiO_4^{4-} can appear as so-called Q^0 to Q^4 units that are charge compensated by Na^+ or Ca^{2+}, for example. In a pure SiO_2 glass, all O^{2-} ions are bound to two Si^{4+} ions (Q^4), forming „bridging oxygens". The introduction of, for example, R_2O alkali ions such as Na_2O forces the net-

GBS	C/S	(C+M)/S	MgO	Al_2O_3	TiO_2	S^{2-}	Na_2O equiv.	NBO/T
	–		wt.-%					–
1	1.14	1.33	6.83	13.6	0.75	0.69	0.74	1.80
2	1.15	1.34	6.94	12.0	0.74	0.63	0.77	1.93
3	1.09	1.26	6.40	9.6	0.61	0.58	0.62	1.98
4	1.14	1.30	6.12	9.4	0.66	0.44	0.61	2.04
5	1.04	1.23	7.32	12.9	0.77	0.71	0.92	1.73
6	1.16	1.35	6.84	11.0	1.79	1.04	0.63	1.96
7	1.14	1.31	6.35	11.5	0.70	0.93	0.65	1.91
8	1.12	1.30	6.84	11.2	1.12	1.08	0.71	1.92
9	1.06	1.23	6.64	11.0	3.02	1.37	0.70	1.78
10	1.10	1.27	6.46	10.1	0.40	1.35	0.79	1.97
11	1.19	1.36	6.30	11.8	0.43	0.97	0.57	1.96
12	1.14	1.32	6.60	11.7	0.70	0.80	0.99	1.93
13	0.86	1.13	10.4	11.2	0.57	0.66	1.44	1.82
14	1.13	1.44	8.36	13.7	1.16	0.79	0.68	1.83
15	0.84	1.17	11.6	20.1	0.78	0.58	0.56	1.30
16	1.02	1.32	11.1	6.8	0.27	0.89	0.48	2.41

Table 1: Chemical composition of the industrial GBS

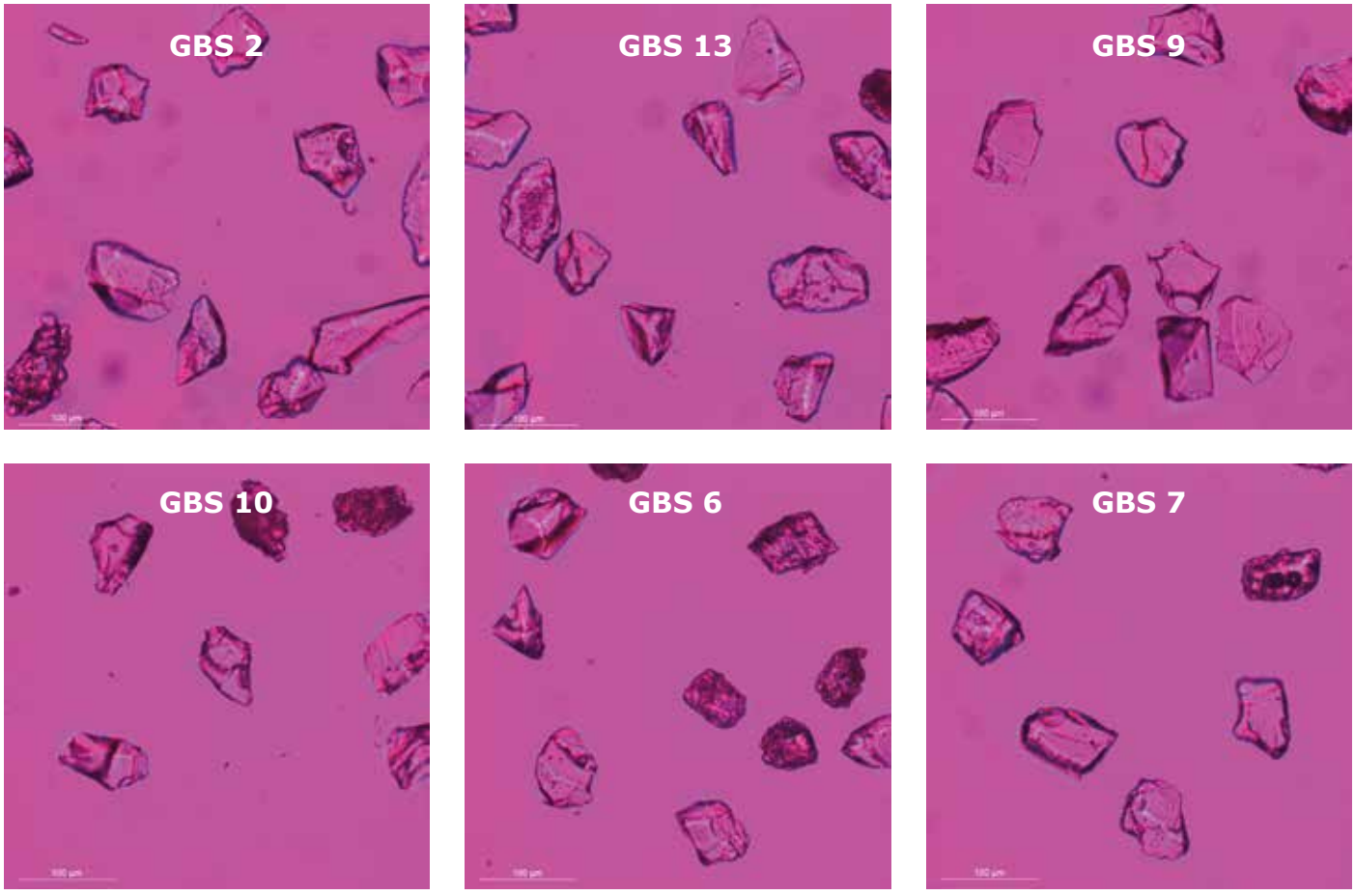

Figure 3: 6 of the 16 industrial GBS (ground fraction 40-63 µm, transmission light microscopy)

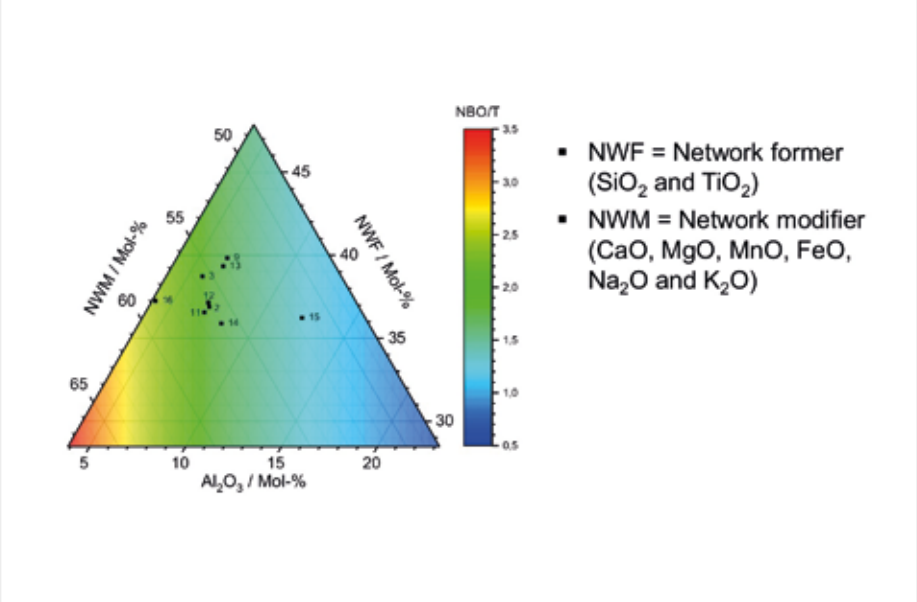

Figure 4: Calculated NBO/T values for GBS 1–16

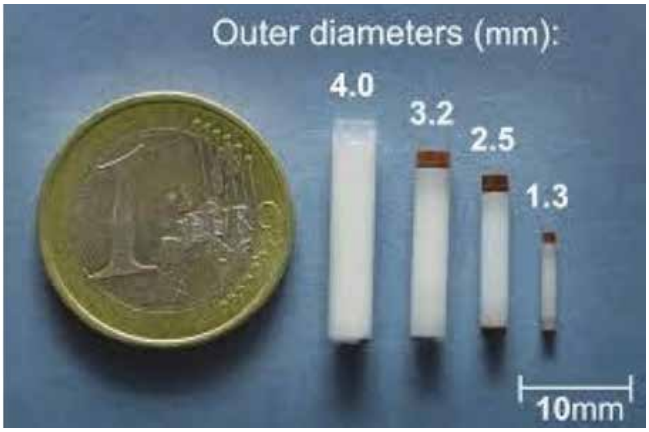

Figure 5: Specimen holders for NMR analyses with ground GBS

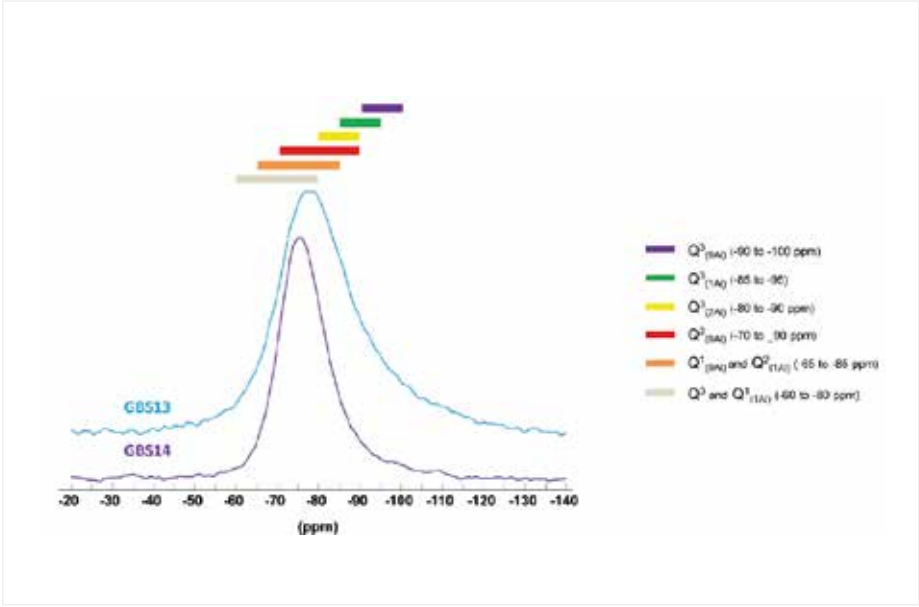

Figure 6: ^{29}Si MAS-NMR spectra for the industrial GBS 13 and 14

work open, resulting in „non-bridging oxygens (NBO)":

$\equiv Si^{4+} - O^{2-} - Si^{4+} \equiv + Na^+ - O^{2-} - Na^+ \rightarrow \equiv Si^{4+} - O^{2-} - Na^+ \mid Na^+ - O^{2-} - Si \equiv$

With increasing introduction of glass network modifications, the coordination is shifted more and more from Q^4 (three-dimensional network) to Q^0 (isolated tetrahedras). From a theoretical point of view, glass forming is impossible for the composition of 2 R_2O-SiO_2. That is an explanation for the experience of lab-scale melting and granulation tests showing that a modified blast furnace slag very high in basicity (CaO/SiO_2) cannot become glassy despite the fact a very effective cooling procedure might be available. For the calculation, the chemical constituents had to be classified into network formers (e.g., SiO_2 and TiO_2), network modifiers (e.g., CaO, MgO, Na_2O and K_2O) and intermediate oxides (Al_2O_3). The TUC calculated the NBO per Si^{4+} tetrahedron ratio (NBO/T) for the different GBS based on the chemical composition (in mol.-%) according to the following equation:

$NBO/T = 2 \times (CaO+MgO+MnO+FeO+Na_2O+K_2O-Al_2O_3)/(SiO_2+TiO_2+2 \times Al_2O_3)$

It must be mentioned that several NBO/T definitions exist that consider more or less chemical constituents. A value of zero would mean that the glass is fully polymerised whereas a value of four would mean that all oxygen is NBO and the structure is fully depolymerised. From a theoretical point of view, a higher NBO/T ratio should result in faster glass corro-

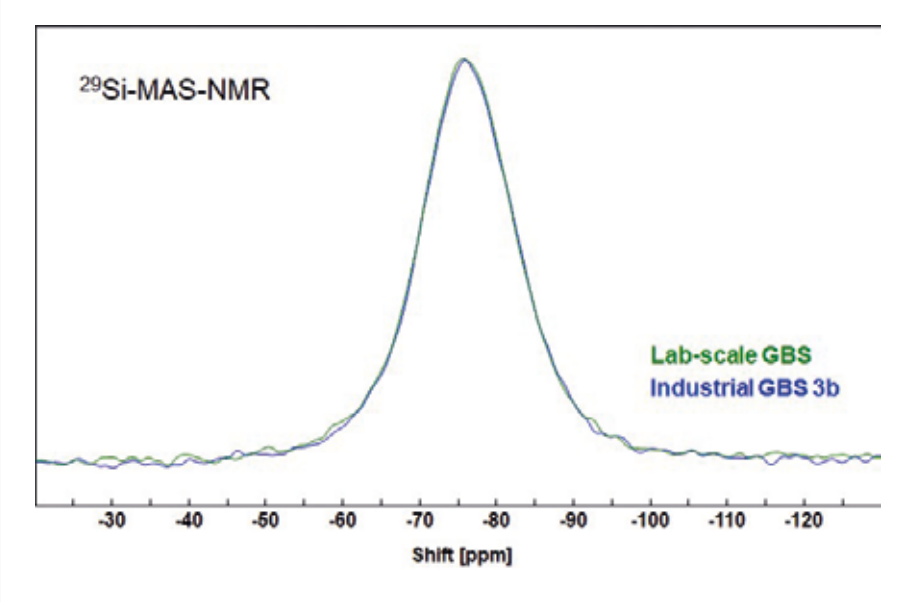

Figure 7: ^{29}Si MAS-NMR spectra for the industrial GBS 3b and the proprietary lab-scale GBS

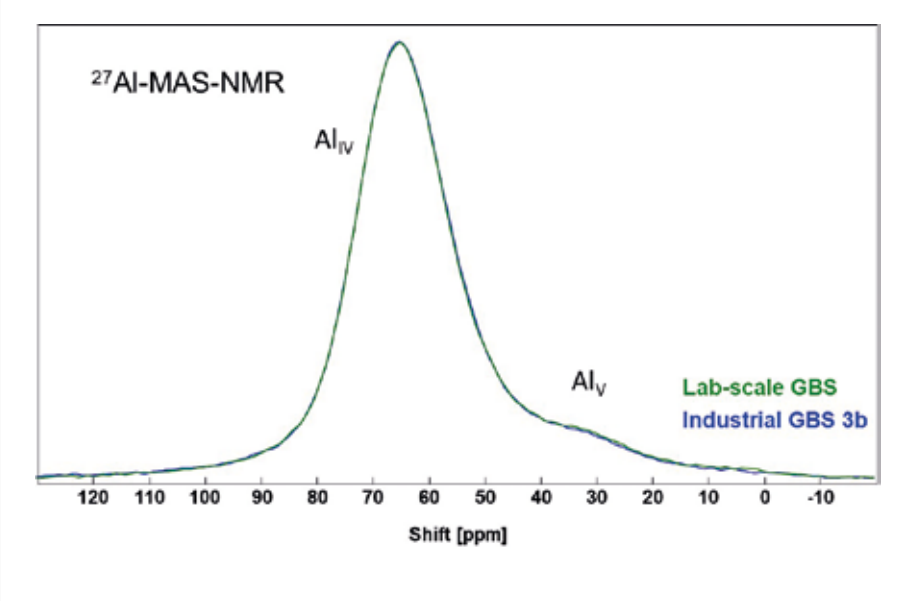

Figure 8: ^{27}Al MAS-NMR spectra for the industrial GBS 3b and the proprietary lab-scale GBS

sion and thus higher GBS reactivity [23, 24, 25].

Most of the NBO/T values were very similar, between 1.82 and 1.92 (Table 1, Figure 4). Thus, all GBS glasses are similar and more depolymerised compared with SiO_2-predominant glass. However, for GBS 15 and 16, significantly lower or higher NBO/T values (1.30 and 2.41, respectively) were calculated due to their very high (GBS 15: 20.1 wt.-%) and very low (GBS 16: 6.8 wt.-%) Al_2O_3 content. A simple correlation between NBO/T and other chemical figures, such as $(CaO+MgO)/SiO_2$, does not exist.

The CEMHTI conducted NMR analyses with ground material. Figure 5 shows the very small specimen holders used (Ø 2.5 mm for Al and Na, Ø 4.0 mm for Si; rotating speed 30 kHz and 10 kHz, respectively). The ^{29}Si MAS-NMR analyses confirm that GBS glasses are not highly polymerised. In most cases, Q^0 - Q^2 groups were detected. Unfortunately, it was not possible to quantify the share of the different Q^x modifications. Figure 6 shows the ^{29}Si spectra for GBS 13 and 14 being very different in basicity (GBS 13: (C+M)/S = 1.13; GBS 14: 1.44). With a higher basicity, the Si coordination shifted more to Q^0. All in all, the NMR analyses confirmed the NBO/T calculations discussed above.

Moreover, for the project, it is important to stress that there is no difference between industrial GBS and samples re-melted on a lab-scale (Figure 7).

The ^{27}Al MAS-NMR analyses show that Al is mainly present in fourfold coordination (Figure 8). Thus, it acts as a glass network former. However, it is well known that a higher Al content increases GBS reactivity, in particular in the early stage. An explanation for this could be that more network modifiers are introduced into the glass matrix to balance the electrochemical equilibration.

Besides glass structural aspects, an important topic of the GBS characterisation was the retroactive measurement of the unknown thermal history in the blast furnace and granulation process. Many years ago, it was already assumed that the thermal history has a relevant impact on GBS reactivity

Fraction:	T_f		T_g	ΔH_{ex}		$\Delta T/\Delta t$		Reactivity ranking
	s	l		s	l	s	l	
GBS	°C			J/g		K/s		–
1	820	800	735	38.6	29.8	4386	540	6
2	839	822	737	43.9	35.5	45905	9276	4
3	837	826	742	41.5	37.3	31140	12120	7
4	838	812	742	43.7	31.4	30705	1983	5
5	827	809	732	42.1	33.4	20607	3258	9
6	828	808	737	42.4	32.6	14167	1773	13
7	820	821	741	35.7	35.8	5890	6555	8
8	822	805	738	39.7	32.3	12681	1902	15
9	823	790	731	44.2	29.0	26626	684	16
10	830	821	736	41.7	37.9	18554	7606	11
11	821	795	743	34.0	21.8	5142	235	1
12	826	787	737	41.5	24.1	12635	144	2
13	809	784	722	28.7	25.9	15163	1188	14
14	838	788	733	53.4	24.5	100000	407	3
15	828	774	729	46.3	20.9	15814	44	12
16	774	768	722	26.7	23.2	298	133	17

Table 2: Results of DSC analyses for industrial GBS (fictive temperature T_f, glass transition temperature T_g, excess enthalpy ΔH_{ex}, small particles "s" 0.355–0.500 mm, large particles "l" 2–4 mm, crushed for DSC analysis); calculation of the temperature-viscosity-correlation according to the MYEGA model [36]

[26]. The general adoption of the so-called „hyperquenching-annealing-calorimetry" approach and the „area-matching method" [15, 16] to GBS was done by the TUC in cooperation with the FEhS. Both the testing and calculating procedures and the problem regarding the selection of representative sub-samples are described in several publications [17, 18, 27, 28, 29]. Table 2 summarises the data for GBS 1–16. It was shown that the thermal history of the industrial GBS differs, as is expected due to different tapping temperatures, heat loss after the tapping hole and granulation facilities. The different cooling histories cannot be reflected by the glass transition temperature T_g due to the test method, which eliminates the original thermal history. Indeed, all T_g values fell within a small range. But the so-called fictive temperature T_f mirrors the real thermal history. The excess enthalpy ΔH_{ex} is an indicator for the thermal driver enabling glassy blast furnace slag to be a latent hydraulic material. It is higher for smaller particles. Thus, granulation facilities should aim to produce glassy particles as small as possible. The calculated cooling rates are extremely high. On the other hand, it is logical that smaller particles „s" have higher cooling rates compared with larger particles „l", and it is known that in larger particles a decline of the cooling rate occurs from the outside to the particle core.

GBS reactivity was tested according to the standard procedure of the FEhS. Most samples were ground in a 10 kg laboratory ball mill to a comparable fineness of about 4,200 cm²/g (Blaine), as shown by the similar RRSB parameters (DIN 66145) d' and n of the particle size distribution, measured by laser granulometry. Thus, any influence of a different fineness on GBS reactivity was avoided. However, for the evaluation of GBS 16, it is important to stress that the average Blaine value of 4,170 cm²/g was influenced by pre-hydration of the slag during storing. The pre-hydration products on the grain surfaces, which are indicated by an increased content of chemical bound H_2O of 0.94 wt.-%, impaired the Blaine test. The $d_{50\%}$- and d'_{RRSB}-values clearly indicate that the ground GBS 16 was coarser compared with other samples. For the 50/50 mixtures, GBS 15 and GBS 16 were not ground in the lab ball mill

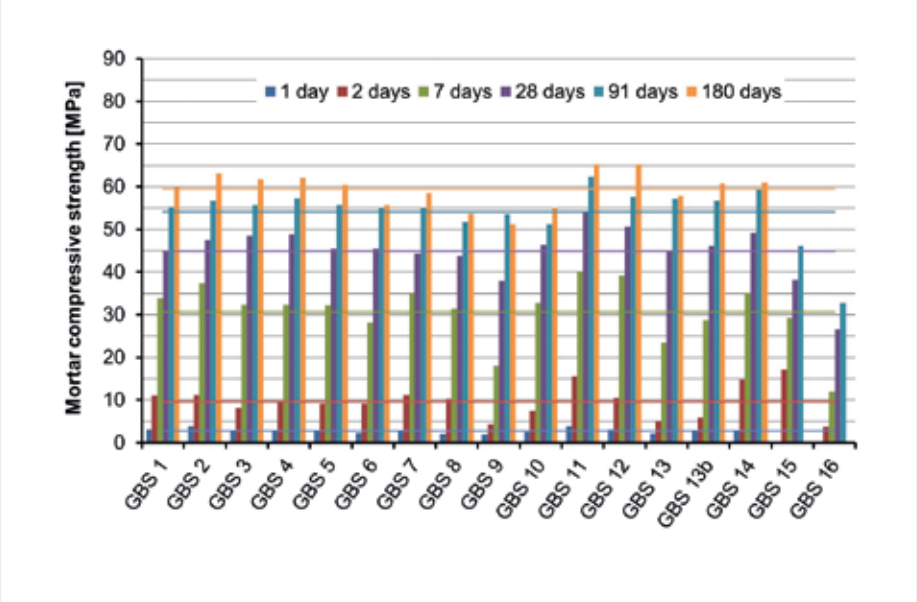

Figure 9: Strength development of blast furnace cements (GBS/Clinker = 75/25) according to EN 196-1

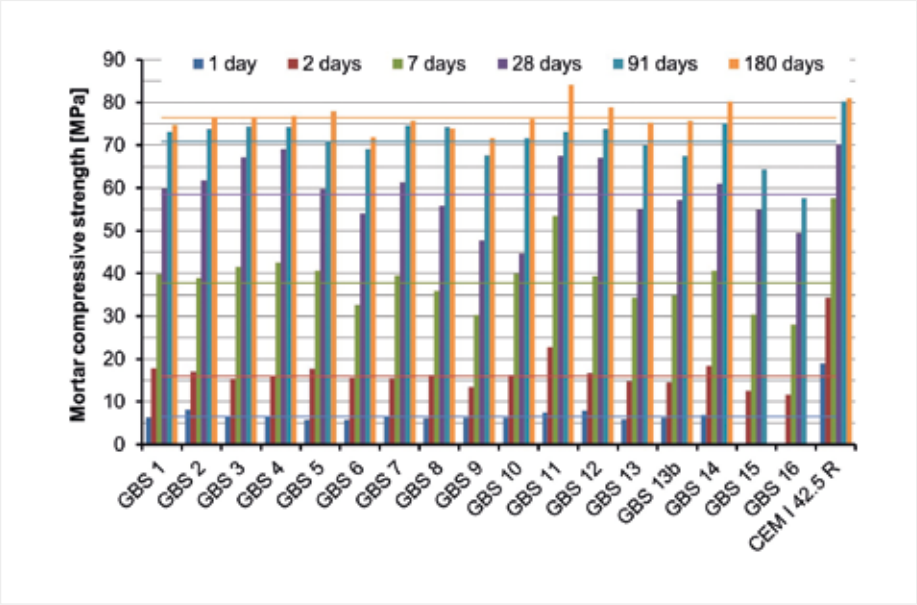

Figure 10: Strength development of blast furnace cements (GBS/CEM I 42.5 R = 50/50) according to EN 196-1

but in a semi-industrial vertical roller mill. Therefore, the slope n of the particle size distribution is higher, which is mainly relevant for the water demand of the cement. Concerning GBS 16, the high Blaine value of 5,490 cm²/g does not correspond to a high fineness (see above). The $d`_{RRSB}$ value shows that only a standard fineness was achieved. Thus, the resulting strength is not overestimated.

Blast furnace cements CEM III/B incorporating 75 wt.-% GBS and 25 wt.-% Portland cement clinker were mixed. A total SO_3 content of 4.5 wt.-% was adjusted by adding a natural ground anhydrite/gypsum mixture. CEM III/B is not the most relevant cement type on the market; however, specific slag properties can be illustrated very well. In addition, mixtures of 50 wt.-% GBS and 50 wt.-% CEM I 42.5 R were mixed according to EN 15167-1. The cementitious properties were tested according to EN 196-1 (mortar strength) and EN 196-9 (heat of hydration) at water/cement ratios of 0.50. Resulting from the wide range of chemical compositions and thermal histories, a wide range of the mortar compressive strengths between 1 and 180 days were measured (Figure 9, Figure 10). Based on these results, 7 GBS were selected to be characterised more in detail by the project partners. Relevant criteria were, for example, a very high (GBS 14) or low (GBS 13) reactivity, similar chemistries, but different granulation facilities (GBS 11, GBS 12) or a very high TiO_2 content (GBS 9).

In general, lower polymerisation (= higher NBO/T) and higher enthalpy (= higher fictive temperature T_f or excess enthalpy ΔH_{ex}) of the GBS glass indicate higher reactivity. However, there is no simple correlation of the glass structure and thermal data with GBS reactivity. The parameters are overlapping. For example, GBS 14 was more reactive compared with GBS 15 with a similar T_f, but had a significantly lower NBO/T value. On the other hand, GBS 14 was more reactive compared with GBS 16 with a much higher NBO/T value, but with a significantly lower T_f.

RAPID TEST DEVELOPMENT

ArcelorMittal Maizières Research was able to carry out a lot of

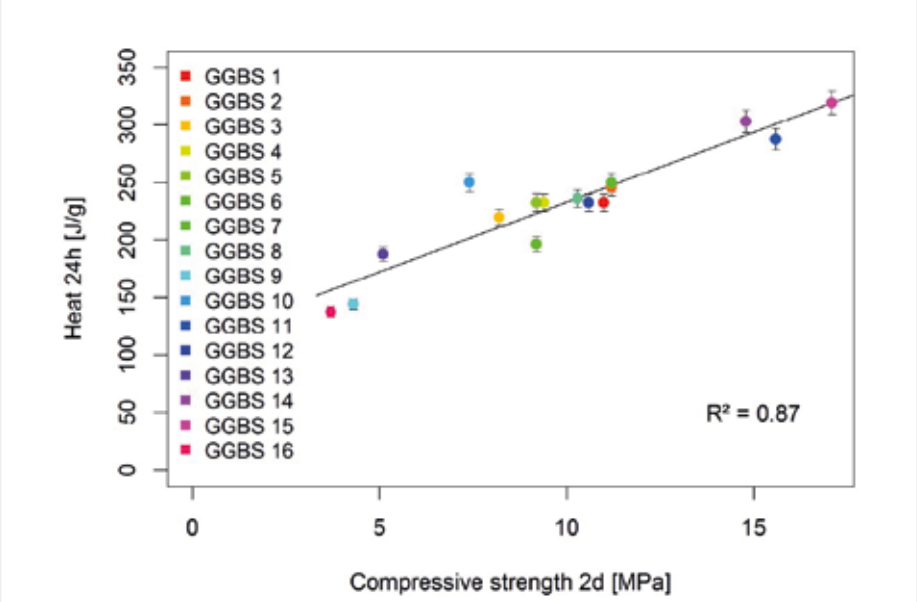

Figure 11: Correlation of heat of hydration after 24 hours according to optimised RILEM R3 test and 2 days mortar compressive strength of slag cements (GBS/Clinker = 75/25) according to EN 196-1 [1]

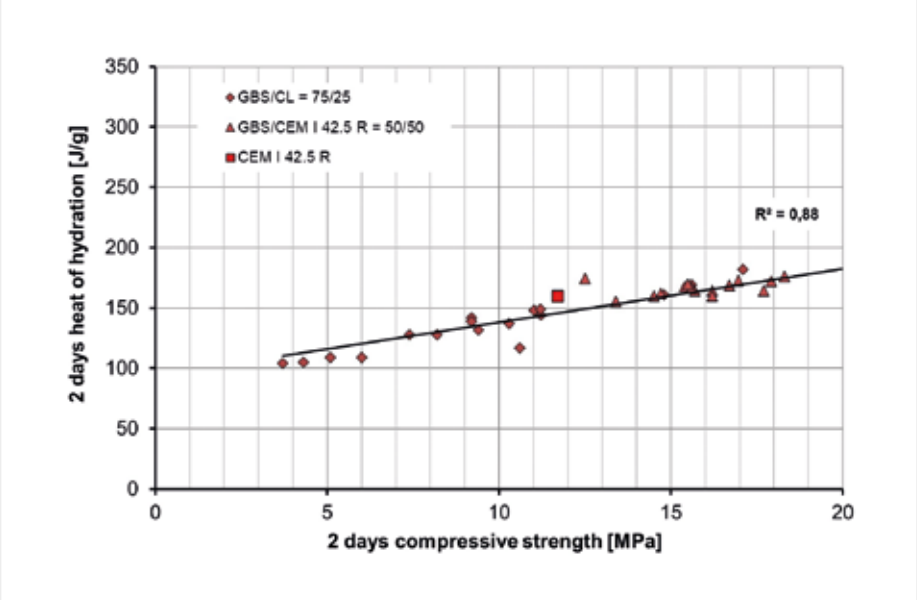

Figure 12: Correlation of heat of hydration after 48 hours according to EN 196-9 and 2 days mortar compressive strength of slag cements (GBS/Clinker = 75/25 and GBS/CEM I 42.5 R = 50/50) according to EN 196-1

lab-scale granulation tests of „upstream activation" by modifying the slag chemistry or the granulation conditions. However, the sample volume was limited, which prevents cement mortar tests according to EN 196-1. Heat of hydration tests according to EN 196-9 with cement lime need only a few grams of material and they normally show a good correlation with mortar strength development, provided that the material system and the physical frame conditions (slag/clinker ratio, fineness, etc.) are kept constant. But this test also normally takes 7 days. To foster the evaluation of the numerous modified slag samples, the LMDC optimised a rapid test based on the RILEM R3 („rapid, reproducible and relevant") test developed as a screening test for any potential supplementary cementitious materials [19]. The test conditions and the results are described in [1]. Table 3 summarises the test conditions. Figure 11 shows that there is a sufficient correlation between the 24 hours heat of hydration of activated GBS measured by the LMDC and the 2 days mortar strength of slag cements with 75 wt.-% GBS measured by the FEhS (Figure 9). This is comparable to the correlation by using the standard test method according to EN 196-9 (Figure 12). It must be stressed that a linear correlation exists only for a limited hydration time. Examination over a longer period (such as from 1 to 7 days) reveals an exponential relationship.

Duration	24 h
Temperature	40°C
GBS	1.5 g
$Ca(OH)_2$	4.5 g
Activator solution: - KOH (0.071 mol/l) - K_2SO_4 (0.115 mol/l)	7.4 ml
w/b	1.23

Table 3: Tests conditions of the optimised RILEM R3 test [1]

EFFECT OF SMALL ADDITIONS TO THE LIQUID BLAST FURNACE SLAG

To realise „upstream activation" by modifying the slag chemistry (main and minor constituents and

Figure 13: Lab-scale granulation facility of ArcelorMittal Maizières Research

glass modifiers) or the cooling procedure (water volume and pressure), ArcelorMittal Maizières Research produced a lot of lab-scale GBS based on the industrial GBS 3. For that purpose, a lab-scale granulation facility was developed (Figure 13) similar to the installation used at the FEhS for many years. Each test produced a sample of about 200 g. Thus, beside the chemical and mineralogical analyses, only heat of hydration tests were possible.

One test program was carried out to produce 16 slags according to a statistical design of experiments. The chemical composition of the lab-scale GBS covered a wide range (CaO: 37-45 wt.-%, MgO: 6-12 wt.-%, Al_2O_3: 8-17 wt.-%, TiO_2: 0.6-2.5 wt.-%). Both the LMDC heat of hydration tests and the strength tests with 2 cm cubes confirm the well-known relationship between the main and minor constituents and slag reactivity. However, the typical high glass content of GBS was not achieved in all lab-scale granulation tests. The main reason for this could be the high crystallisation velocity of blast furnace slags being very high in basicity.

Another test program investigated the influence of very small additions of potential glass modifiers to the liquid slag. Based on experiences with other glasses [30], the effect of, for example, BaO, Cr_2O_3 or ZrO_2 was analysed [3]. The basic idea was to weaken the glass structure to enable faster dissolution. However, Table 4 shows that in nearly all cases no or a negative impact was observed. Compared with the re-melted industrial GBS 3, the 24 hours heat of hydration (modified R3 test) was mostly decreased. According to the LMDC results, the strongest negative impact came from ZrO_2 (-51 %), followed by Cr_2O_3 (-21 %). The latter constituent is of particularly high inte-

Addition	Concentration		$HoH_{24\ hours}$
	wt.-%	as	J/g
Industrial GBS 3 (re-melted)	-	-	212
ZrO_2	5.1	ZrO_2	104
Cr_2O_3	1.3	Cr_2O_3	168
CeO_2	1.9	CeO_2	178
MnO	2.9	MnO	195
$Ca_3(PO_4)_2$	1.1	P_2O_5	202
SnO_2	1.2	SnO_2	214
SrO	1.8	SrO	215
Cs_2CO_3	0.2	Cs_2O	218
BaO	2.0	BaO	220
K_2CO_3	1.2	K_2O	233

Table 4: Heat of hydration of modified lab-scale GBS after 24 hours according to the optimised RILEM R3 test

	GBS 4	Acti 1	Acti 2	Acti 3	Acti 6	
SiO_2	37.0	36.3	36.3	36.4	34.8	wt.-%
Al_2O_3	10.4	9.83	9.53	9.50	9.61	
TiO_2	0.66	0.65	0.77	0.71	**2.01**	
CaO	42.1	45.7	44.4	44.1	45.4	
MgO	6.12	6.51	6.32	6.28	6.45	
Na_2O	0.40	0.09	0.17	0.17	0.16	
K_2O	0.32	**0.09**	**1.36**	**2.09**	0.15	
Na_2O equivalent	0.61	**0.15**	**1.07**	**1.54**	0.26	
S_{total}	0.65	0.72	0.70	0.71	0.67	
S^{2-}	0.44	0.69	0.56	0.62	0.59	
C+M+S	85	89	87	87	87	wt.-%
C/S	1.14	1.26	1.22	1.21	1.30	-
(C+M)/S	1.30	1.44	1.40	1.38	1.49	
Glass	96.6	-	-	-	99.7	vol.-%

Table 5: Chemical composition of lab-scale GBS based on industrial GBS 4 (red: intended modifications)

	GBS 4	Acti 1	Acti 2	Acti 3	Acti 6	
SiO_2	34.1	33.7	31.9	26.2	27.2	wt.-%
Al_2O_3	9.40	**14.0**	**18.7**	**20.5**	**19.7**	
TiO_2	0.69	0.69	0.65	0.50	0.58	
CaO	44.5	43.5	41.4	**44.3**	**46.2**	
MgO	**9.37**	6.19	5.90	4.62	5.14	
Na_2O	0.12	0.18	0.18	0.19	0.13	
K_2O	0.11	0.18	0.18	**2.20**	0.10	
Na_2O equivalent	0.19	0.30	0.30	**1.63**	0.19	
S_{total}	0.65	0.64	0.59	0.46	0.44	
S^{2-}	0.56	0.61	0.59	0.45	0.92	
C+M+S	88	83	79	75	79	wt.-%
C/S	1.30	1.29	1.30	**1.69**	**1.70**	-
(C+M)/S	**1.58**	1.47	1.48	**1.87**	**1.89**	
Glass	99.5	100.0	99.8	99.3	98.8	vol.-%

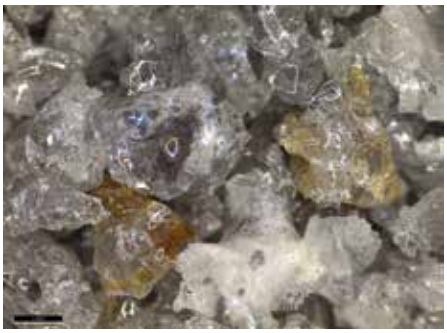

Acti 3 with 2.09 wt.-% K_2O

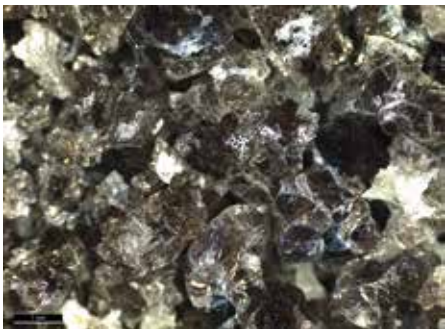

Acti 6 with 2.01 wt.-% TiO_2

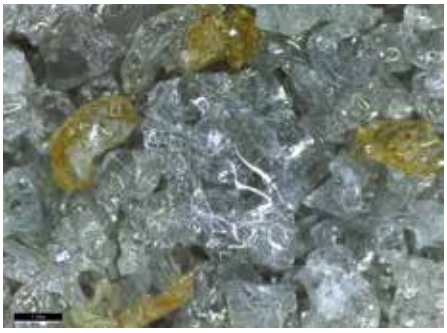

Acti 10 with 20.5 wt.-% Al_2O_3, 2.20 wt.-% K_2O, C/S = 1.69

Acti 12 with 19.7 wt.-% Al_2O_3, C/S = 1.70

Figure 14: Some lab-scale granulated GBS based on industrial GBS 4

rest. The strategy of the steel industry to substitute the CO_2 intensive blast furnace process with a combination of direct reduction and electrical melting may result in slags with higher contents of heavy metals, such as chromium [35], so far scrap has been melted together with DRI. Thus, a negative impact on slag reactivity must be considered if both the new slags and the common fully scrap-based EAF slags should be used for cementitious purposes in the future. A limited promising result has come from the K_2CO_3 addition (+10 %). Thus, the increase of K_2O is one of the tasks for the FEhS described in the next chapter.

„UPSTREAM MODIFICATION" BY ADJUSTING THE SLAG CHEMISTRY

In the melting laboratory of the FEhS, the industrial GBS 4, which is very similar to GBS 3, was mixed with correction materials and the mixtures were re-melted in a Tammann furnace in carbon crucibles at 1,550°C (furnace temperature). The liquid slags were water granulated with a water flow of 70 l/min. Two melts (each about 2 kg) were produced for every mixture. The general melting and granulation procedure is described in, for example, [31]. All melts had a low viscosity. Furthermore, Acti 10, with its high basicity, was still a thin fluid due to the increased Al_2O_3 content. Besides the chemical and mineralogical analyses (FEhS) and the heat of hydration tests (FEhS, LMDC), the higher sample volume enabled the project partners to also test mortar strength (FEhS), thermal history (TUC) and glass structure (CEMHTI).

Table 5 summarises the chemical composition of some modified GBS. Acti 1 is the re-melted GBS 4 without any modification in order to eliminate potential lab-scale re-melting and granulation effects. Based on the results described above, Acti 2 and 3 had higher K_2O contents. To avoid foaming, instead of K_2CO_3, a K_2O-SiO_2 potassium-metasilicate glass provided by the TUC (61.2 wt.-% K_2O) was used. The K_2O content changed from 0.32 wt.-% in the original GBS, only 0.09 wt.-% in the re-melted slag (evaporation effect), to 1.36 wt.-% and 2.09 wt.-%, respectively. Acti 6 had a higher TiO_2 content (2.01 wt.-% instead of 0.65 wt.-%) in order to verify the well-known negative impact on GBS reactivity. In Acti 7, the basicity (CaO+MgO)/SiO_2 was increased by adding only MgO (1.58 instead of 1.44). Acti 8 and 9 had significantly higher Al_2O_3 contents (14.0 wt.-% and 18.7 wt.-%, res-

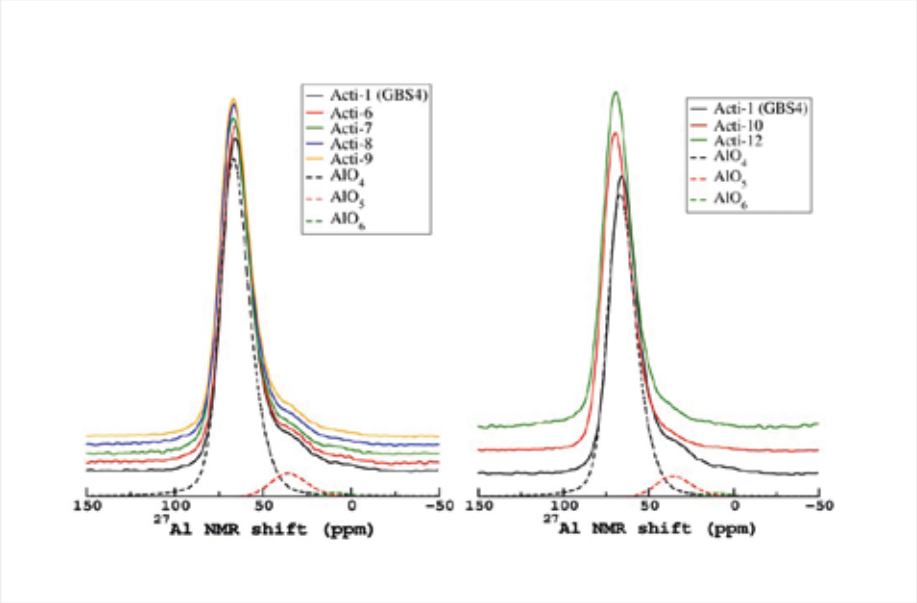

Figure 15: ^{27}Al MAS-NMR spectra recorded at 19.9 T with a spinning rate of 30 kHz for different modified lab-scale GBS (Acti 1 is the re-melted industrial GBS 4)

	T_f	T_g	ΔH_{ex}
	C°		J/g
GBS 4	838	742	43.7
Acti 1	842	754	-
Acti 2	839	744	-
Acti 3	(862)*	744	-
Acti 6	841	749	39.7
Acti 7	842	748	40.9
Acti 8	852	756	42.0
Acti 9	876	763	47.7
Acti 10	886	768	45.4
Acti 12	872	773	38.5

** over-estimated due to problems with cp1 measurement*

Table 6: Results of DSC analyses for lab-scale GBS based on industrial GBS 4 (only fraction "s" 0.355–0.500 mm)

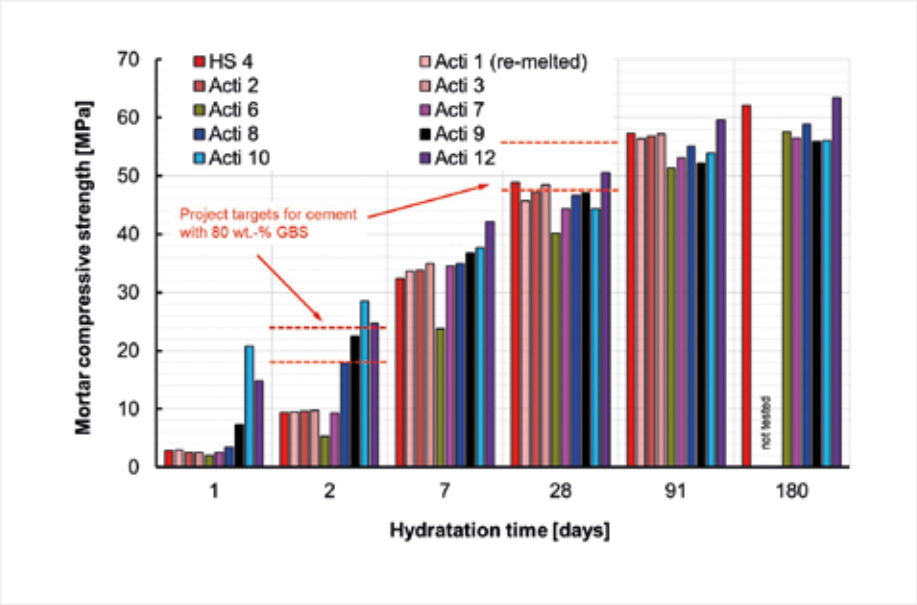

Figure 16: Strength development of blast furnace cements (GBS/Clinker = 75/25) made with different modified lab-scale GBS

pectively, instead of 9.8 wt.-%). For Acti 10 and 12, different chemical optimisations were combined. Figure 14 shows some examples of the lab-scale GBS. Acti 6 had the typical dark colour of GBS enriched in TiO_2.

The DSC analyses of the TUC show that the chemical modification of the slags resulted both in different glass transition temperatures T_g and fictive temperatures T_f (Table 6). For example, the Al_2O_3 addition in Acti 9, 10 and 12 increased T_g from 742°C for the industrial GBS 4 to 763–773°C. That is a clear indication that the glass network stabilizing (!) impact of Al_2O_3 is in line with the ^{27}Al MAS-NMR spectroscopy results of the CEMHTI confirming that in GBS mainly

	GBS 4	Acti 1	Acti 2	Acti 3	Acti 6	
Density	2.944	2.946	2.935	2.934	2.964	g/cm³
Blaine	4240	4150	4290	4220	4230	cm²/g
d`$_{RRSB}$	15	17	16	17	18	µm
n	0.92	1.01	1.07	1.09	0.97	-

	Acti 7	Acti 8	Acti 9	Acti 10	Acti 12	
Density	2.951	2.931	2.919	2.916	2.952	g/cm³
Blaine	4190	4240	4420	4340	4180	cm²/g
d`$_{RRSB}$	16	16	15	16	17	µm
n	1.06	0.97	0.94	1.04	1.08	-

Table 7: True density and fineness parameters of ground lab-scale GBS based on industrial GBS 4

fourfold coordinated Al (AlO_4^{5-}) exists (from 90 mol.-% in Acti 1 to 97 mol.-% in Acti 12), acting as a network former (Figure 15). On the other hand, the difference of about 2 wt.-% K_2O in Acti 10 and Acti 12, respectively, corresponds to a ΔT_g of 5°C. Furthermore, the lack of K_2O in Acti 1 (= re-melted GBS 4) due to the evaporation effect during the re-melting process decreased T_g by about 10°C compared with GBS 4 and Acti 2 and 3.

In general, the NBO/T ratio was increased. As discussed earlier, higher NBO/T ratios correspond to a more depolymerised glass network. The ^{29}Si MAS-NMR analyses of the CEMHTI showed that the Si environment was not changed by introducing TiO_2 (Acti 6) or Al_2O_3 (Acti 8 and 9). Changes were, however, seen in Acti 7 (higher MgO content), Acti 10 (higher basicity and K_2O content) and Acti 12 (higher basicity). The latter shifted to a more depolymerised structure.

For the cement tests, the re-melted GBS was ground to the FEhS standard fineness. The relevant parameters are given in Table 7. Due to the limited sample volume, in some cases the lab-scale GBS was a little less fine compared with the industrial GBS 4. This must be considered if the strength development of the slag cements is compared.

Figure 16 shows the strength development of the slag cements made with 75 wt.-% GBS. The influence of the significantly increased K_2O content is low (Acti 2 and 3). The significantly negative TiO_2 impact was confirmed (Acti 6). MgO does not have the same positive effect as CaO, also if it is evaluated equitably in the basicity definition used for GBS as a cement constituent (EN 197-1) or concrete addition (EN 15167-1). Higher Al_2O_3 contents significantly foster early strength, despite Al_2O_3 being mainly coordinated fourfold (see above). All in all, it can be concluded that the ambitious early strength target of the project was achieved by using classical chemical „upstream activation". The strengths after 28 days were comparable and on the same level. Through limited increasing of the slag fineness, the 28 days strength might be increased to a sufficient degree.

THE NEGATIVE TIO_2 IMPACT

The LMDC performed a lot of hydration and characterisation tests and „downstream activation" investigations, which are described in detail, for example in [1, 2, 3, 6]. One additional aspect was to investigate the well-known negative impact of increased TiO_2 contents (> 1 wt.-%) on GBS reactivity [5]. To explain the negative TiO_2 effect [32], several earlier studies have referred to a stabilised glass structure. In [23], it was stated that both the Ti^{4+} (instead of Si^{4+}) and Ti^{3+} (instead of Ca^{2+}) tighten the glass network. In [32], it is mentioned that a Ti^{4+} content above 1 mol.-% increases glass polymerisation. A contracting effect was also described. Indeed, the true density of GBS increases with a higher TiO_2 content (compare Acti 1: 2.946 g/cm³ with Acti 6: 2.964 g/cm³ in Table 5). In [33], the results of electron paramagnetic resonance (EPR) spectroscopy and X-ray absorption near-edge structure (XANES) spectroscopy were discussed. EPR allows differentiation of Ti^{3+}, Ti^{4+}, etc., and XANES allows determination of their coordination numbers. According to these investigations, the dominant species is Ti^{4+} (67%), but Ti^{3+} is also present (33%). Ti^{4+} was mainly five- and fourfold coordinated and acts as network former. Most of the oxygen ions are bridging oxygens. In addition, for charge compensation, Ca^{2+} is bound due to the limited availability of Na^+ ions. Hence, in the SiO_4^{4-} network,

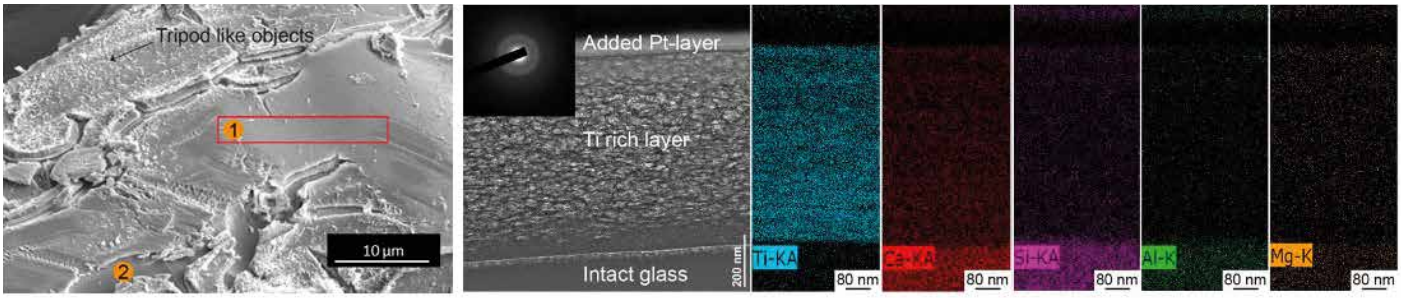

Figure 17: SEM (left) image and for area 1 the TEM image and elemental maps for a model glass grain (3.1 wt.-% TiO_2) after 14 days of exposure to pH = 11 (NaOH solution) [5]

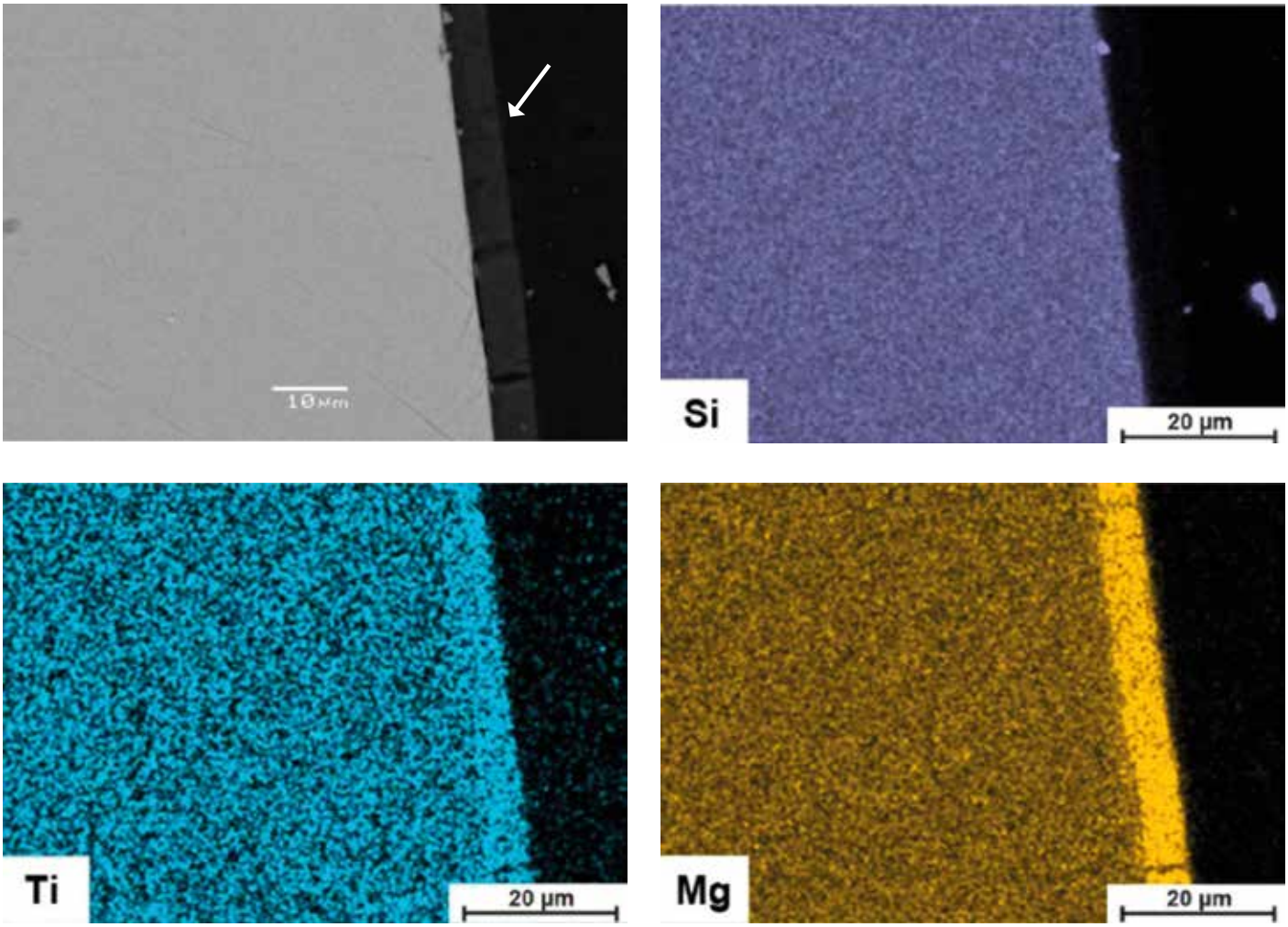

Figure 18: SEM image and elemental maps for a modified granulated slag grain (2.4 wt.-% TiO_2) after 10 days of exposure to pH 13 (NaOH solution) [5]

Ca^{2+} is no longer available as a glass network modifier. The fivefold coordination is independent on the TiO_2 content of the glass.

To complete the review, it must be mentioned that rotating viscometer tests with liquid slags showed a viscosity decreasing (!) effect if TiO_2 was increased up to 5 wt.-% [34]. Raman spectroscopy confirmed a depolymerising effect. This seems to be a contradiction to the glass structure strengthening effect described above. On the other hand, these tests were done with slags with 17 wt.-% Al_2O_3, which is much

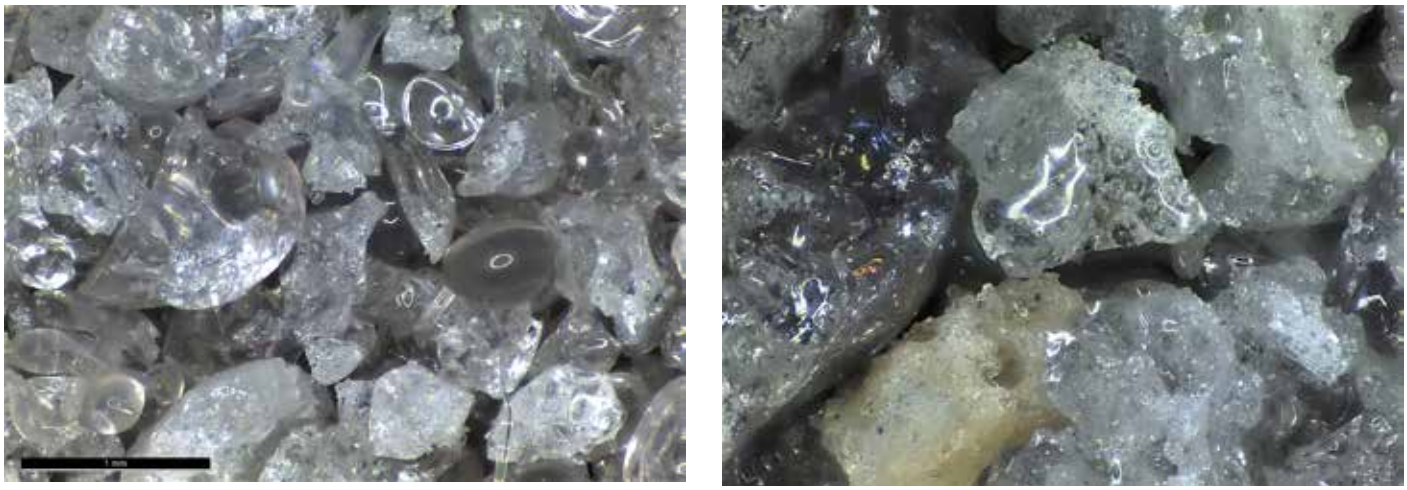

A139 with 6 m³/h

A145 with 2 m³/h

Figure 19: Two lab-scale granulated GBS with different granulation water flows based on industrial GBS 3

higher compared with today's European blast furnace slags (Table 1). Furthermore, it is known that Al_2O_3 significantly influences slag viscosity, which was also demonstrated by Acti 10.

Within „ActiSlag", the effect of TiO_2 additions up to 3.1 wt.-% in model glasses and modified GBS has been studied by the LMDC in terms of glass structure and glass dissolution in an alkaline environment (pH = 11 and 13). SEM, TEM, EDS, EPR, and XANES were used. The expensive latter test was carried out at the SOLEIL synchrotron in Saint-Aubin, France. All methods and results are described in detail in [5].

Figure 17 shows the surface of a ground (fraction 40-80 µm) model glass grain (TiO_2 = 3.1 wt.-%) after 14 days at pH = 11 (NaOH solution). An amorphous surface layer of about 1 µm was formed (Figure 17, left). The result of the EDS analysis for point 1 was 44.6 wt.-% TiO_2 instead of only 4.5 wt.-% for point 2 (crack). TEM/EDS analyses of a vertical slice of the glass grain (area 1) attest to a significant Ti enrichment (TiO_2 = 66 wt.-%), as shown in the centre of Figure 17.

A similar surface layer was found after corrosion tests at pH = 13. Figure 18 shows SEM pictures for an unground modified GBS grain (TiO_2 = 2.4 wt.-%) after 10 days at pH = 13 (NaOH solution). It is obvious that the surface layer was enriched in Ti and Mg, whereas the Si, Ca and Al contents were depleted. From the grain core (left) to the surface layer, the TiO_2 content increased from 2.6 wt.-% to 18.3 wt.-% and the MgO content from 6.3 wt.-% to 37.6 wt.-%.

The XANES analyses of the unreacted ground glass samples identified fourfold, fivefold and sixfold coordinated Ti ions. The share of the dominant fivefold coordination was calculated to be about 70% and the share of fourfold coordination was calculated to be about 30%, whereas sixfold coordination was not relevant. Thus, the results confirmed the results described in the literature [33]. The XANES analyses for the surface layer of reacted glass samples were very different compared with the unreacted glass samples or the core of reacted glass grains. According to these, about 50% fivefold coordination and 50% sixfold coordination was found. The results for the tests carried out at pH = 11 and 13 were comparable.

Based on the confirmed glass structure strengthening effect of a higher TiO_2 content, it was expected that the different dissolution tests would show big differences. However, the dissolution rates decreased only by 10%–28% which does not explain the significant loss in GBS reactivity measured according to the R3 method described above [5]. Thus, it is presumed that in real cementitious systems, newly formed hy-

	Water flow	Glass	< 0.5 mm	T_f	T_g	ΔH_{ex}	$\Delta T/\Delta t$	HoH	
								48 h	96 h
	m³/h	vol.-%	wt.-%	°C		J/g	K/s	J/g	
GBS 3	-	99.9	35	837	742	41.5	$0.3 \cdot 10^5$	179	230
A139	6	100.0	51	855	747	41.8	$2.7 \cdot 10^5$	176	225
A140	5	99.9	30	852	748	41.2	$2.0 \cdot 10^5$	174	222
A141	4	99.9	23	841	748	38.7	$0.8 \cdot 10^5$	173	220
A142	3	100.0	12	837	747	36.9	$0.6 \cdot 10^5$	172	219
A145	2	99.8	9	835	747	36.3	$0.5 \cdot 10^5$	176	224

Table 8: DSC (only fraction "s" 0.355–0.500 mm) and heat of hydration data (EN 196-9; GBS/CEM I 42.5 R = 50/50) for lab-scale GBS with varied granulation conditions compared with industrial GBS 3

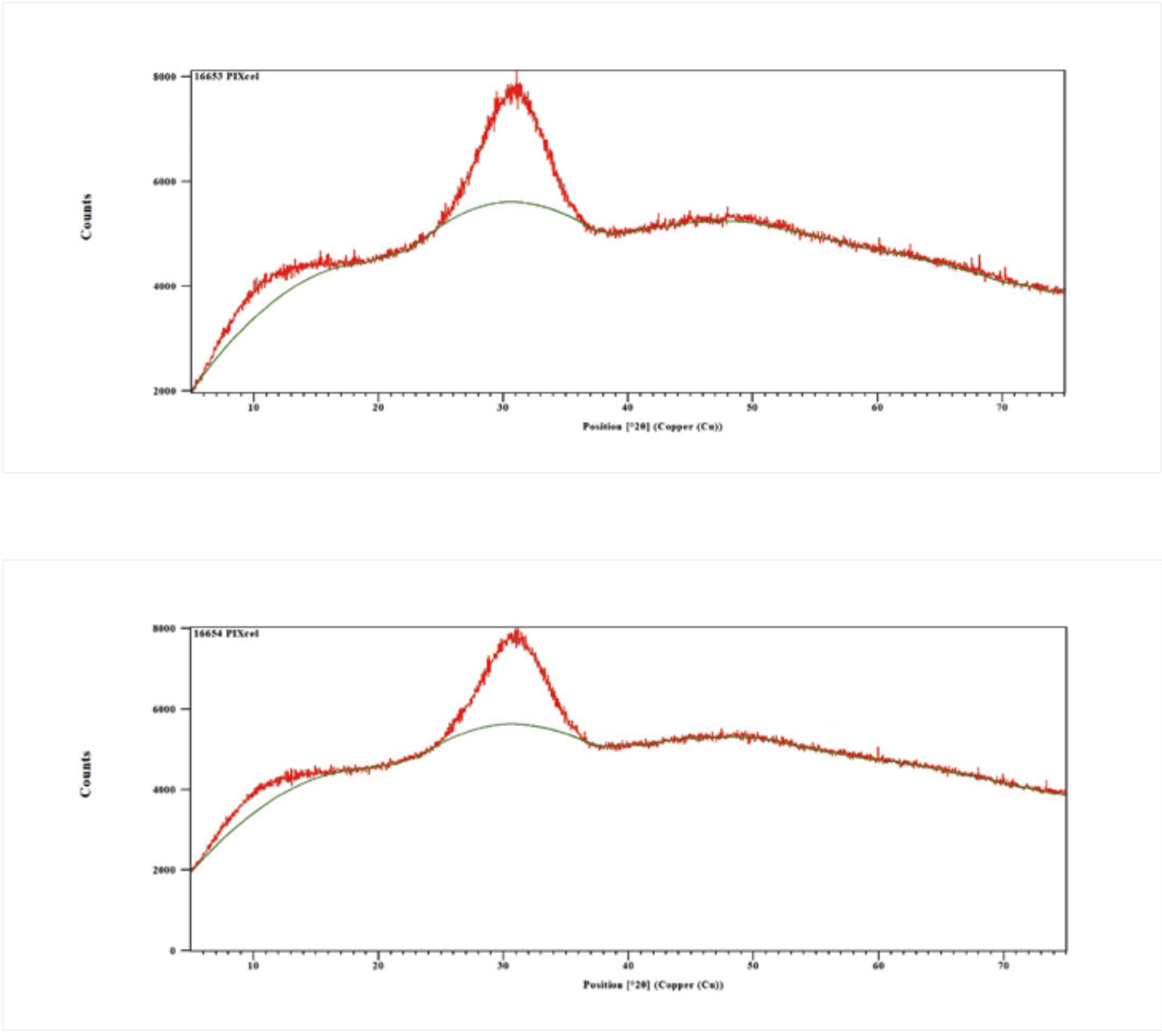

Figure 20: XRD for lab-scale GBS A142 (above) and GBS A145 (below)

dration products such as hydrotalcite ($Mg_6Al_2 \cdot 4\ H_2O$) precipitate in the porous Ti-rich surface layer resulting in a densifying, passivating and thus glass dissolution-hindering effect. Therefore, the negative impact of increased TiO_2 content on GBS reactivity is not explainable by only one effect.

INFLUENCE OF COOLING CONDITIONS

Besides the chemical composition, the granulation conditions (i.e., water flow rate) were also varied in lab-scale granulation tests carried out by ArcelorMittal Maizières Research. A higher water flow resulted in finer and less porous particles (Figure 19). The glass contents were similar and very high (Figure 20). Table 8 summarises the test conditions and the thermal parameters analysed by the TUC for the fraction „s" (0.355–0.500 mm). As expected, there is no relevant change for T_g due to the unchanged chemical composition of the lab-scale GBS. However, a higher water flow rate resulted in higher values for T_f and ΔH_{ex}. The calculated cooling rate increased from $05 \cdot 10^5$ K/s at 2 m^3/h to $2.7 \cdot 10^5$ K/s at 6 m^3/h. Thus, from a theoretical point of view, the lab-scale GBS produced with higher cooling rates should be more reactive.

To verify this assumption, the FEhS conducted some heat of hydration tests according to EN 196-9 for a combination of 50 wt.-% GBS and 50 wt.-% CEM I 42.5 R with a water/cement ratio of 0.50. Due to the very limited sample volume, the five lab-scale GBS were ground in a vibration mill instead the 10 kg ball mill to a comparable fineness (3,710–3,790 cm^2/g according to Blaine, $d`_{RRSB}$ = 17–18 µm). Therefore, the industrial GBS 3 was also ground in the vibration mill (4,200 $cm^2/g$, $d`_{RRSB}$ = 14 µm). As the heat of hydration values show (Table 8), no significant change was measured. There is only a slight negative heat of hydration tendency for the samples A139–A142 in parallel to their decreasing cooling speed. However, neither a different fineness nor a different glass content can explain the result for sample A145 with the lowest cooling speed. It might be that the cooling rates and the thermal data for all lab-scale GBS indeed differed, but at a very high level and in a lower range compared with industrial GBS (Table 2). Thus, the variation could be too small for a significant reactivity influence. It seems that the impact of the chemical composition and the glass structure is higher compared with the cooling conditions, if an intensive cooling process and a high glass content are assured.

OUTLOOK

„ActiSlag" was focused on classical GBS as it has been produced and used for cementitious purposes for decades. If the steel production transformation process is realized, starting in Europe, step-by-step blast furnaces will be substituted with a combination of direct reduction and electrical melting processes, based on green hydrogen and green electrical power. Thus, the well-known GBS will vanish, too. Nevertheless, the project results also have great relevance for new slags. These slags will differ compared with today's GBS to some degree [35]. However, it is a clear target for steel and slag producers to further enable these slags for utilisation in

cement and concrete to ensure the environmental (lower raw material and primary energy demand, lower CO_2 emission) and technical (high durability) advantages of slag-containing cements. Therefore, the „ActiSlag" results regarding the influence of chemical or thermal parameters on glass structure and reactivity, the hydration process, and the efficiency of accelerating additions are also transferable to new slags.

ACKNOWLEDGEMENT

The RFCS project 749809 „New activation routes for early strength development of granulated blast furnace slag (ActiSlag)" has been funded by the European Union, represented by the European Commission, Directorate General Research & Innovation. The project partners express their thanks for the financial support.

Moreover, the author gives thanks for the excellent cooperation with the project partners and many fruitful discussions. <<<

Co-funded by the European Union

LITERATURE

[1] Blotevogel, S. et al.: Ability of the R3 test to evaluate differences in early age reactivity of 16 industrial ground granulated blast furnace slags (GGBS). Cement and Concrete Research 130 (2020) 105998 https://doi.org/10.1016/j.cemconres.2020.105998
[2] Steger, L. et al.: Experimental evidence for the acceleration of slag hydration in blended cements by the addition of $CaCl_2$. Cement and Concrete Research 149 (2021) 106558 https://doi.org/10.1016/j.cemconres.2021.106558
[3] Blotevogel, S. et al.: Effect of TiO_2 and 11 minor elements on the reactivity of ground-granulated blast-furnace slag in blended cements. Journal of the American Ceramic Society 104 (2021) 1, 128-139 https://doi.org/10.1111/jace.17431
[4] Blotevogel, S. et al.: Glass structure of industrial ground granulated blast furnace slags (GGBS) investigated by time-resolved Raman and NMR spectroscopies. Journal of Materials Science 56 (2021) 17490–17504 https://doi.org/10.1007/s10853-021-06446-4
[5] Blotevogel, S. et al.: Titanium in GGBS-like calcium-magnesium-aluminosilicate glasses: Its role in the glass network, dissolution at alkaline pH and surface layer formation. Journal of Non-Crystalline Solids 591 (2022) 121708 https://doi.org/10.1016/j.jnoncrysol.2022.121708
[6] Poitier, M. et al.: Synchroton X-ray micro-tomography investigation of the early hydration of blended cements: A case study on $CaCl_2$-accelerated slag-based blended cements. Construction and Building Materials 321 (2022) 126412 https://doi.org/10.1016/j.conbuildmat.2022.126412
[7] Danezan, A. et al.: Study of the kinetic of hydration of industrial granulated blast furnace slags: A structural investigation. 6th Int. Slag Valorisation Symposium, Mechelen, 2019
[8] Hart, D. et al.: Cooling rate and reactivity of granulated blast furnace slag. 1. Joint Meeting Deutsche Glastechnische Gesellschaft and Union pour la Science et la Technologie Verrières, Nuremberg, 13.05.2019
[9] Danezan, A. et al.: Solid state NMR investigation of titanium's role on the hydration of industrial slags: A model glass study. 10th European Slag Conference, Thessaloniki, 2019
[10] Kaknics, J. et al.: ActiSlag - New activation routes for early strength development of granulated blast furnace slag. 10th European Slag Conference, Thessaloniki, 2019
[11] Danezan, A. et al.: Induced effect of titanium on the reactivity of industrial blast furnace slag: a model glass study. 14th Int. Conference on the Structure of Non-Crystalline Materials, Kobe, 2019
[12] Ehrenberg, A.: ActiSlag - New activation routes for early strength development of granulated blast furnace slag."REUsteel" webinar, 14.06.2021
[13] Kaknics, J. et al.: „ActiSlag" webinar, 31.01.2022
[14] Kaknics, J. et al.: ActiSlag - New activation routes for early strength development of granulated blast furnace slag. 11th European Slag Conference, Cologne, 2022
[15] Yue, Y. Z., Christiansen, J., Jensen, S. L.: Determination of the fictive temperature for a hyperquenched glass. Chemical Physics Letters 357 (2002) 1/2, 20-24 https://doi.org/10.1016/S0009-2614(02)00434-7
[16] Guo, X. et al.: Unified approach for determining the enthalpic fictive temperature of glasses with arbitrary thermal history. Journal of Non-Crystalline Solids 357 (2011) 3230-3236 https://doi.org/10.1016/j.jnoncrysol.2011.05.014
[17] Pronina, N. et al.: Cooling history of a wet-granulated blast furnace slag. Journal of Non-Crystalline Solids 499 (2018) 344-349
[18] Ehrenberg, A. et al.: Glass structure of granulated blast furnace slag and its reactivity - A new approach. 6th Int. Slag Valorisation Symposium, Mechelen, 2019
[19] Li, X., Snellings, R., Scrivener, K.: RILEM TC 267-TRM Committee: RILEM TC 267-TRM report: Results of a round robin campaign on chemical reactivity test methods for supplementary cementitious materials. 15th Int. Congress on the Chemistry of Cement, Prague, 2019
[20] Drissen, P.: Determination of the glass content in granulated blastfurnace slag. Zement-Kalk-Gips 48 (1995) 1, 59-62
[21] Ehrenberg, A. et al.: Granulated blastfurnace slag: Reaction potential and production of optimized cements. Cement International 6 (2008) 2, 90-96 (part 1), 3, 82-92 (part 2)

[22] Scholze, H.: Glass - Nature, structure, and properties. New York, 1991
[23] Olbrich, E., Frischat, G. H.: Corrosion of granulated glassy blast furnace slags in aqueous solutions. Glass Science and Technology, 74 (2001) 4, 86-96
[24] Wolter, A., Frischat, G. H., Olbrich, E.: Investigation of granulated blast furnace slag (GBFS) reactivity by SNMS. 11th Int. Congress on the Chemistry of Cement, Durban, 2003
[25] Schöler, A. et al.: The effect of glass composition on the reactivity of synthetic glasses. Journal of the American Ceramic Society 100 (2017) 6, 2553-2567 https://doi.org/10.1111/jace.14759
[26] Schröder, F.: Blastfurnace slags and slag cements. 5th Int. Congress on the Chemistry of Cement, Tokyo, 1968
[27] Ehrenberg, A., Romero Sarcos, N., Hart, D., Bornhöft, H., Deubener, J.: Glass formation of granulated blast furnace slag and its influence on slag reactivity. Report of the FEhS – Institute für Baustoff-Forschung 1 (2019) 1, 26-32
[28] Ehrenberg, A., Romero Sarcos, N., Bornhöft, H., Deubener, J.: Influence of the thermal history of granulated blast furnace slags on their latent-hydraulic reactivity in cementitious systems. Journal of Sustainable Metallurgy 6 (2020) 2, 207-215
[29] Ehrenberg, A., Romero Sarcos, N., Hart, D., Bornhöft, H., Deubener, J.: The thermal history of granulated blast furnace slag and its impact on reactivity. ZKG International 72 (2020) 4, 30-39
[30] Hujová, M., Vernerová, H.: Influence of fining agents on glass melting: A review, part 1. Ceramics-Silikáty 61 (2017) 2, 119-126
[31] Ehrenberg, A.: Granulated blast furnace slag - Lab-scale investigations vs. reality. 5th Int. Slag Valorisation Symposium, Leuven, 2017
[32] Wang, Z. P., Rudert, V., Lang, E., Trettin, R.: Influence of the TiO_2 content on the reactivity of granulated blastfurnace slags. Cement International 1 (2002) 1, 120-128
[33] Le Cornec, D. et al.: Structural role of titanium on slag properties. Journal of the American Ceramic Society 104 (2021) 1, 105-113 https://doi.org/10.1111/jace.17407
[34] Park, H., Park, J.-Y., Kim, G. H., Sohn, I.: Effect of TiO_2 on the viscosity and slag structure in blast furnace type slags. Steel Research 83 (2012) 2, 150-156 https://doi.org/10.1002/srin.201100249
[35] Ehrenberg, A.: The steel production transformation process - consequences for the slag utilization. 11th European Slag Conference, Cologne, 2022
[36] Mauro, J.C., Yue, Y., Ellison, A.J., Gupta, P.K., Allan, D.C.: Viscosity of glass-forming liquids. Proceedings of the National Academy of Sciences of the United States of America 106 (2009) 19780–19784

Find us on social media

Imprint // **Editor:** FEhS – Building Materials Institute // **Responsible:** Thomas Reiche, Managing Director // **Layout:** del din design

FEhS – Building Materials Institute
Bliersheimer Straße 62
47229 Duisburg
Germany

Telephone: +49 2065 9945-0
Fax: +49 2065 9945-10
E-Mail: fehs@fehs.de
www.fehs.de

INSTITUT FÜR
BAUSTOFF
FORSCHUNG